Proiect InnoRESEARCH - POSDRU/159/1.5/S/132397
Burse doctorale și postdoctorale în sprijinul inovării și competitivității în cercetare

UNIVERSITATEA „POLITEHNICA” din BUCUREȘTI
ȘCOALA DOCTORALĂ ETTI-B
Nr. Decizie 168 din 24.11.2017

PhD THESIS

SUMMARY

Technological improvements for sensors and MEMS

Author: **Ing. Angela-Mihaela Băracu**

EXAMINATION COMMITTEE

President of the Committee	**Prof. Ion Marghescu**	from	**Univ. Politehnica Bucharest**
Thesis Supervisor	**Prof. Gheorghe Brezeanu**	from	**Univ. Politehnica Bucharest**
Adviser	**Prof. Lidia Dobrescu**	from	**Univ. Politehnica Bucharest**
Adviser	**Dr. Raluca Müller**	from	**NIRD for Microtechnologies**
Adviser	**Dr. Adrian Dinescu**	from	**NIRD for Microtechnologies**

BUCUREȘTI 2017

Contents

CHAPTER 1

INTRODUCTION

1.1 Thesis research field

The PhD thesis "Contributions to the Technological Development of Sensors and MEMS Structures" is a synthesis of the main directions approached during this study, highlighting the obtained scientific results. The first important topic in my research activity was the development of surface acoustic wave devices (SAW-Surface Acoustic Waves).

The way of acoustic wave propagation at the surface of a piezoelectric substrate was for the first time described by Lord Rayleigh in 1885 [1]. Later, in 1965, White and Voltmer found a method to generate and receive acoustic waves by using interdigital transducers (IDTs) [2]. Since then, acoustic surface waves have been used for a wide range of applications: the telecommunications industry, automotive applications (tire pressure sensors), medical (chemical and bio sensors), industrial and commercial (humidity sensors and temperature sensors). The telecommunications industry is the main consumer of such components, providing an annual consumption of about 5 billion SAW filters [3].

Another important topic developed in my thesis was related to the technological development of micro-electro-mechanical structures (MEMS-MicroElectroMechanical Systems).

MEMS technology has been developed progressively, after Charles Smith's piezoresistive effect, at Bell Laboratories in 1954 [4]. A year later, there were publications describing the first piezoresistive pressure sensor. Since then, the most successful commercial applications of MEMS have been pressure sensors. Demand in this area has increased from about 3 million units in 1983, to more than 50 million units in 1995 and is expected to increase to over 125 million units per year in the following years. At the same time, raising public awareness of healthcare, physical activity and safety, has generated a growing demand for intelligent sensor technologies and monitoring devices, fabricated with MEMS systems.

1.2 Thesis research objectives

The aim of this thesis is to propose configurations and technological optimization solutions for SAW sensors and MEMS structures.

The main activities developed for reaching this purpose consisted in developing chemical sensors using surface acoustic wave devices, proposing MEMS structures configurations and adjusting technological processes for the devices performance optimisation. SAW-structures for chemical sensors, electro-thermal MEMS actuators for radio-frequency switches and micro-cantilevers for vibration sensor applications were designed and manufactured.

Special attention was paid to the structural materials characterisation and devices testing, using a system that allow structures measurement on the wafer. The chemical sensors are the only structures excepted from the wafer-level testing. They were first packaged and tested using the vector network analyser, for the detection of the mycotoxin in a liquid environment,

The development of technological processes for SiC micromachining (for MEMS structures) was another important objective of this work. The critical step for SiC micromachining was dry reactive-ion etching.

CHAPTER 2

MICROSENSORS AND MEMS ACTUATORS

2.1 SAW devices for sensor applications

Wohltjen and Dessy were the first who report a gas sensor based on a SAW structure, in 1979, using Rayleigh Surface Sound Waves (RSAW). The key element of the gas chemical sensor was the sensitive polymeric material which reacts with the organic gas target. Ever since, there have been many approaches in the field of SAW sensors, used for a variety of applications [5]. Since 1980, SAW devices have proven to be suitable for many applications, mainly in electronics and high-frequency technology.

A main advantage of surface acoustic wave devices for sensor applications is the low cost due to manufacturing technology. These devices are obtained using the planar technology of integrated circuits. Considering the advantages of SAW devices used for sensor applications, in this thesis there will be designed, manufactured and tested a SAW based chemical sensor architecture for mycotoxin detection.

2.2 MEMS devices with electro-thermal and electrostatic actuation

The first MEMS device used to receive radio signals was developed by Harvey C. Nathanson in 1965. Six years later, a refined version of the device was patented as a resonant gate transistor [6]. In his work on developing similar devices, Nathanson presented a method of manufacturing in batches, in which the insulating and metallic layers at the top of the silicon wafer were configured by using masks and sacrificial layers. This method subsequently became the essential element of manufacturing of MEMS systems [7].

The development of MEMS structures and micro-nano-electronics technologies in recent years has allowed both miniaturization and integration into many applications. The MEMS miniaturized, high sensitivity, integrable, and therefore portable, with highly flexible responses have a major impact on human society, being present in more and more products that are necessary for daily existence: sensors in airbags, sensors for measuring wheel pressure, micro-mirrors for video projectors, medicine: controlled drug delivery or smart phones.

Depending on the field of application, MEMS have different modes of operation. Within this thesis there will be designed and implemented two classes of micro-electro-mechanical systems: (i) electro-thermal MEMS devices and (ii) electrostatic actuated MEMS structures.

Electro-thermally actuated MEMS operate according to the Joule effect (the physical phenomenon of a conductor heating when passing electric current through it). Electrostatically actuated structures use the electrostatic attraction force between two objects charged with different electrical charges.

The manufacture of MEMS devices is accomplished using the classical surface and bulk micromachining technology.

CHAPTER 3

SAW DEVICES FOR CHEMICAL SENSOR APPLICATIONS

Using interdigitated transducers (IDTs) on the piezoelectric crystal surface, SAW devices can generate and detect acoustic waves. Therefore, the acoustic energy is concentrated on the structure's surface in the acoustic wavelength range, regardless of the piezoelectric substrate thickness. Acoustic waves are very sensitive to changes occurring at the surface of the crystal, such as mass variations, viscosity or conductivity.

3.1 SAW sensor configuration

The proposed SAW structure has the configuration of a delay line (Fig. 3.1). Device configuration consists of two IDTs patterned on a piezoelectric substrate (quartz, lithium tantalate or langasite). When a radio frequency voltage is applied, the input transducer generates an acoustic wave in the piezoelectric substrate, which travels to the output IDT. Using the piezoelectric effect, the wave is converted back into an electric signal via output IDT.

For SAW devices used in sensor applications, the acoustic wave velocity changes are correlated to the equivalent physical quantity that you intend to measure. Using the propagation velocity in the piezoelectric substrate of the SAW device, the resonant frequency can be determined by the following relationship:

$$f_r = \frac{v_p}{\lambda} = 4 \cdot d \tag{3.1}$$

where v_p is the propagation velocity of the wave, λ is the wavelength and d is the interdigital transducer width.

The design data (Fig.3.1) was chosen according to the 121 MHz central frequency of the structure, for the $LiTaO_3$ piezoelectric substrate. The IDTs have 50 finger pairs each, organised in single-finger configuration, with λ=34 μm electrode width. The fingers are placed at λ/4 = 8.5 μm one to the other. The IDT aperture is W=70λ (2.38 mm) and the spacing between interdigital transducers is l=100λ=3.40 mm, for D= 50λ=5.10 mm center to center IDT separation. The sensing area is 9 mm2 (3 mm × 3 mm).

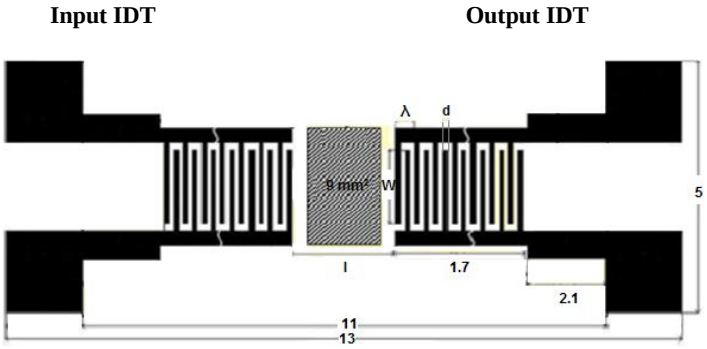

Fig. 3.1 *Design parameters of the SAW chemical sensor [8]*

3.2 Photolithographic masks design

The chemical sensor fabrication required the use of three photolithography masks. The design was done using dedicated CleWin program [9]. The masks design was achieved according by the following stages of the technological flow:

- *Lift-off process in order to obtain the iterdigital transducers (IDT);*
- *Silicon dioxide deposition, used as guiding layer;*
- *Metal film deposition (Cr/Au) and detection area defining;*

- *Windows opening in the SiO_2 layer using wet etching process to achieve the pad device access;*

The first photolithography mask was used in order to pattern the two IDT metal structures. The configuration of this mask is illustrated in Fig. 3.2.

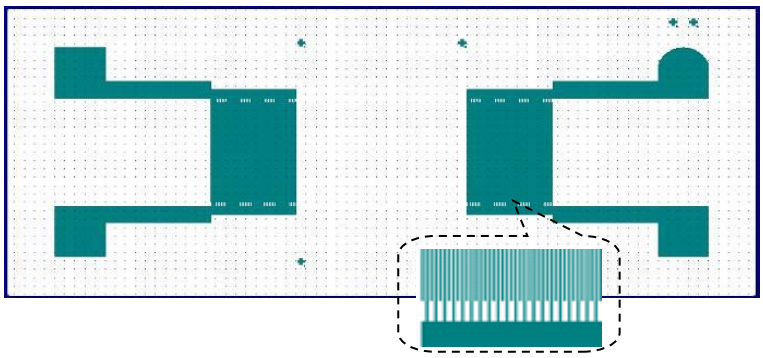

Fig. 3.2 *Photolithography mask for interdigital transducers patterning*

The next step in the technological flow was the deposition of SiO_2 over metal interdigital structures. This layer reduces the wave attenuation in $LiTaO_3$.

The following technological step was the Cr/Au metal film deposition for the patterning of the detection area. Consequently, the second photolithography mask has the role to delimit and retain the metal only on the active surface, Fig. 3.3.

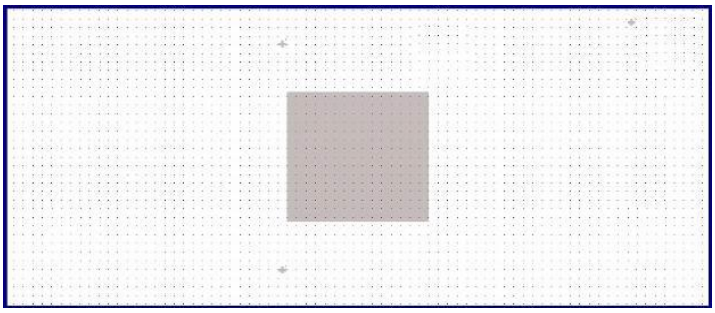

Fig. 3.3 *Photolithography mask for detection area patterning*

After etching process, the selected area from the photolithography mask will remain coated with metal. The last mask was designed to uncover the pad shape of the structure. In Fig 3.4 is illustrated the mask number 3 used for SAW chemical sensor pads patterning.

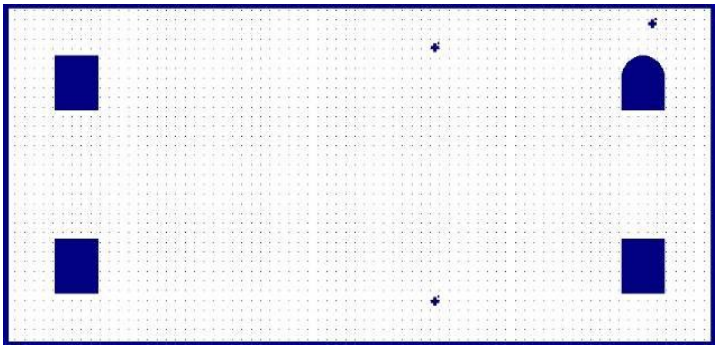

Fig. 3.4 *Photolithography mask for chemical sensor pads patterning*

That mask will be transparent in the coloured areas and opaque to the rest. This polarity ensures the unlocking of the device's metal pad.

An overview of the three overlaid masks can be seen in Fig. 3.5.

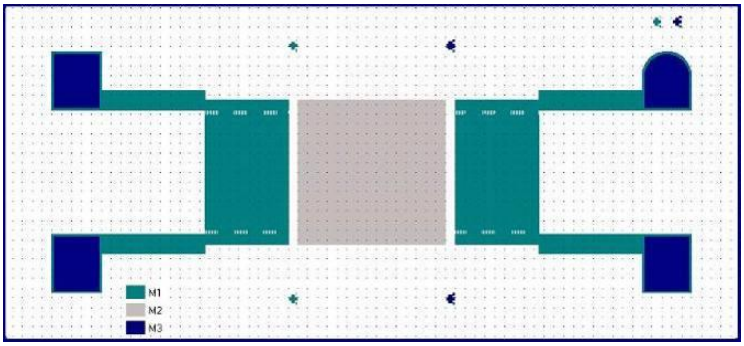

Fig. 3.5 *Overview of the three overlaid designed masks*

3.3 Technological fabrication of SAW structures

The SAW chemical sensor has been fabricated on $LiTaO_3$-36^0YX piezoelectric substrate; the surface acoustic wave propagates along X axis with particle movement in the Y-Z plane. In this case the SAW sensor must be positioned on the piezoelectric substrate according to the Fig. 3.6.

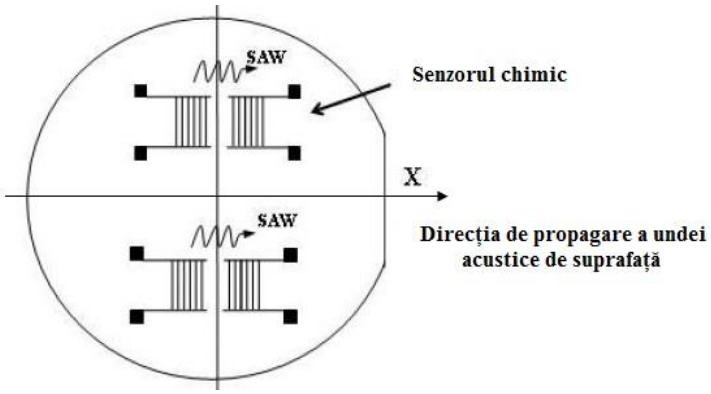

Fig. 3.6 *The SAW sensor positioning on the $LiTaO_3$ substrate*

The propagation surface is optically polished with an average square value R_{rms} = 0.66 nm and the opposite face is lapped, having a mean roughness R_a = 0.3 μm. In this piezoelectric substrate, according to the crystal cut, SH-SAW guided waves appear.

- ***Chemical cleaning of $LiTaO_3$ wafers***

The major disadvantage of commercially available SH-SAW chemical sensors is the utilization of Al for IDTs fabrication. This metal significantly reduces cost devices, but limits the operating time due to the corrosion occurrence. The combination of Cr/Au metals has been chosen just to eliminate this effect.

To obtain a high dimensional control of IDTs, the lift-off technique has been used. This technological stage involves the use of the first photolithographic mask according to the following steps:

- *Az 5214 positive photoresist layer deposition (3000 rpm);*
- *Thermal treatment at T = 90ºC for30 min.;*
- *Expose photoresist using M1 mask;*
- *Exposed photoresist developing;*
- *Metal films evaporation: 10 nm thickness Cr, used as adhesion layer and 100 nm thickness Au, used as structural material;*
- *Photoresist layer removal together with the metal on its surface;*

The interdigital transducers configuration was obtained following the steps outlined above. The optical and SEM profile of the IDT elements can be seen in Fig. 3.7.

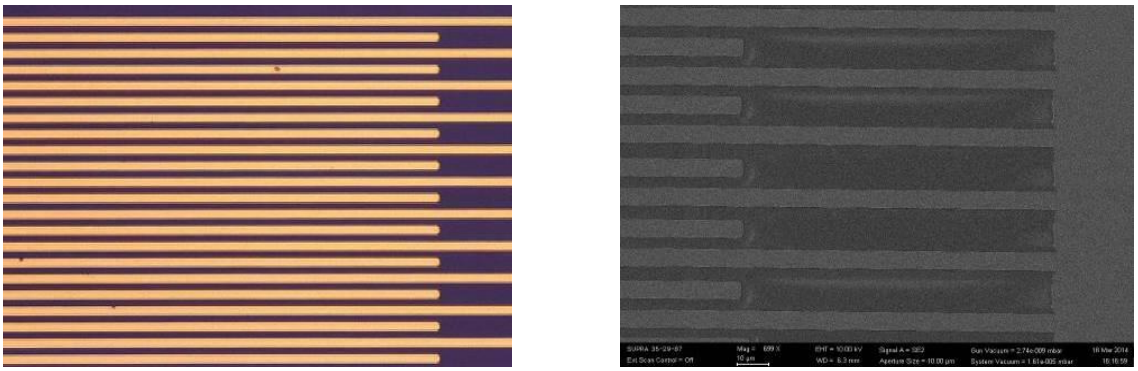

(a) (b)

Fig. 3.7 *The IDT elements profile: (a) Optical şi (b) SEM [10].*

- ***Guiding layer deposition of the chemical sensor***

To increase the device sensitivity, because the acoustic wave goes deeper into the substrate, a layer of silicon dioxide (2 μm thickness) deposited by PECVD has been chosen as waveguiding material. The acoustic wave propagation velocity in this material (2850 m/s) is much lower than in the $LiTaO_3$ piezoelectric substrate (4112 m/s), which makes it suitable for the proposed application [11]. In addition, the SiO_2 layer deposited over the already patterned IDTs ensures the elements isolation.
Due to the pyroelectric phenomenon present in the $LiTaO_3$ substrate, the SiO_2 layer has been deposited using PECVD method, which offers the advantage of low temperature deposition (200-400ºC).

- ***The patterning of SAW sensor detection area***

After IDTs covering with silicon dioxide, a new Cr/Au metallic film (10/100 nm thickness) has been deposited by the evaporation technique in order to define the detection area. This was patterned using the second photolithography mask. The technological process is described by the following steps:

- *HPR 504 positive photoresist layer deposition (3000 rpm);*
- *Thermal treatment at T = 90ºC for30 min;*
- *Expose photoresist using M2 mask;*
- *Exposed photoresist developing;*
- *Thermal treatment at T = 90ºC for30 min;*
- *Wet etching of the metals;*
- *Photoresist layer removal;*

The metal etching process began with the removal of Au in a chemical solution based on Iodine, Potassium Iodide, Ethyl Alcohol and Deionized Water and heated to 40°C. Using the same photolithography mask, by immersing the wafers in a solution based on cerium and ammonium nitrate, perchloric acid (HClO4) and deionized water, the Cr film was selectively removed.

- ***The patterning of pads SAW sensor***

In order to provide the access to the SAW device pads, that will be contacted by Au wires in the packaging process, the oxide that masks the corresponding areas must be removed. For this purpose, the third photolithographic mask has been used, according to the following technological processes:

- *HPR 504 positive photoresist layer deposition (3000 rpm);*

- *Thermal treatment at T = 90ºC for30 min;*
- *Expose photoresist using M3 mask;*
- *Exposed photoresist developing;*
- *Thermal treatment at T = 90ºC for30 min;*
- *Wet etching of the SiO_2;*
- *Photoresist layer removal;*

The SiO_2 etching was performed using a chemical solution, called BOE, composed of ammonium fluoride (NH_4F) and hydrogen fluoride (HF), in a ratio of (6: 1) and maintained at a temperature of 22°C. The etching rate of the PECVD deposited oxide in this solution is 200 nm/min. Sensor technology flow ended with $LiTaO_3$ wafer dicing.

3.4 Packaging process

To encapsulate the fabricated structures for their use as chemical sensors, there was used a Ni metallic package, with four terminals insulated by means of glass inserts (pillars) supporting the terminals. The frequency behaviour of this type of capsule is very good because the glass has low losses [12], and the length of the pads crossed by metallic terminals is only 1.5 mm. The electrical connection of the chip with the package was done in this way:

- *The chip has been glued to the Ni package with Ag conductive paste;*
- *Connections between the chip pads and the package terminals were realised using gold wires, with a diameter of 25 μm;;*
- *The encapsulated chip was thermal treated at 150ºC, for 90 min;*

Fig. 3.8 (a) illustrates how to connect a chip to the Ni package, and in Fig. 3.8 (b) one can be seen, in detail (SEM), the pad connection at the terminals of the package by Au-wires.

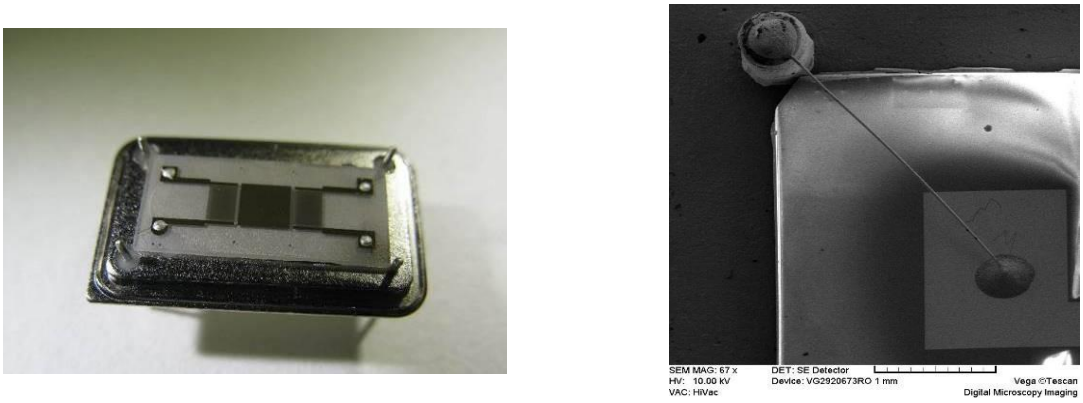

(a) (b)

Fig. 3.8 *SAW chemical sensor packaging: (a) Chip bonding; (b) Pad connection to the package terminals [10]*

3.5 Sensor's functional testing

The measurement system needs to be well calibrated in order to have a good precision of the measurement results, even if the sensor's working frequency is small (115-130 MHz). This will lead to the minimization of the unavoidable influences of several circuit elements within the test structure: the length of the connectors and/or the dedicated adaptors, the influence of the adapters from one connector type to another, the length and attenuation of the connection cables or the influence of other elements [13].

The vector network analyser Anritsu 37397D, available in IMT, uses SOLT-type calibration (lines terminated with short and open circuit, transmission line segment and adapted termination). The calibration components, designed and fabricated for the package model used for the SAW sensor encapsulation, are presented in Fig. 3.9. Also, the chosen model of package connection in the circuit

does not introduce other parasite/supplemental circuit elements as compared to the original calibration model. This provides the advantage of a very good precision and minimal corrections to the already measured network parameters values.

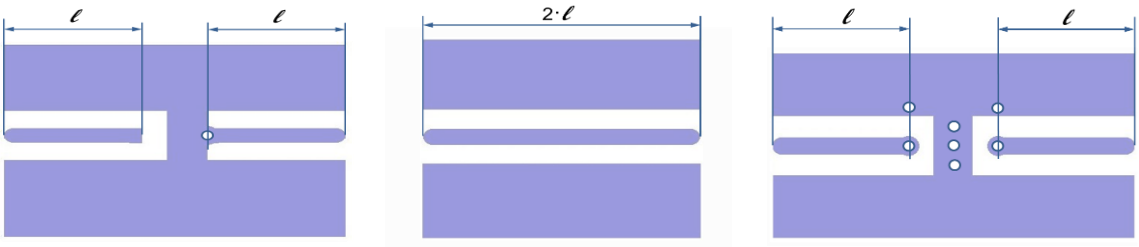

(a) (b) (c)

Fig. 3.9 *The calibration structures in (1) open and short circuit, (b) transmission line and (c)the measurement setup, provided with a socket for the SAW device package insertion*

The calibration components set is made of transmission lines with the same characteristic impedance, Z_0:

- *Two transmission lines with equal electric lengths l, one of which is terminated in an open circuit, the other one is terminated in a short circuit;*
- *One transmission line with 2·l electrical length, provided with connectors at both ends.*

This description refers to the electrical length of the transmission line instead of its physical length, because for the open circuit terminated line, a correction (shortening) of the line is needed in order to compensate for the terminal capacitance of the line in open circuit (for which there are simple analytical relations [14], [15]). Another correction can be applied to the short circuit terminated line, especially if the working frequency is large, because the inductance of the metallised holes between the end of the transmission line and the ground, which constitute this termination, cannot be neglected for the microstrip lines.

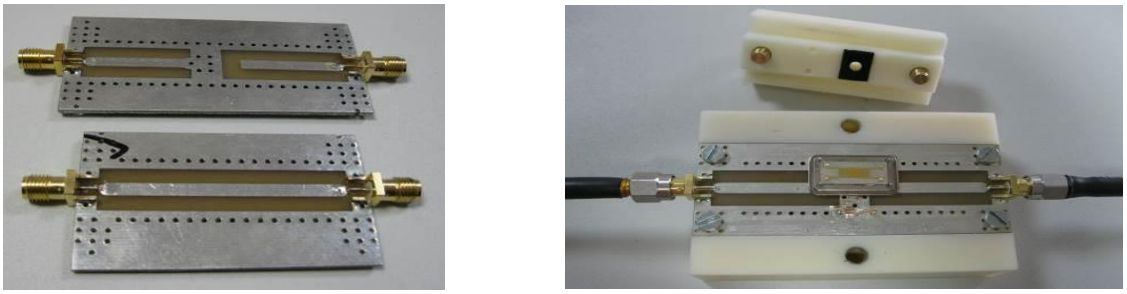

(a) (b)

Fig. 3.10 *(a) Calibration structures and (b) The measurement setup with the inserted SAW device [8]*

The average working frequency of the sensor is around 120 MHz; therefore, the applied corrections are 0.37 mm for the open circuit terminated line and 0.2 mm for the short circuit terminated line, respectively.

The device was functionally tested, using the measurement setup with the package connected in the circuit, as shown in Fig. 3.10. The measured network parameters describe the device's behaviour at the package's terminals. The SAW structures were used for the immune-sensors development, for mycotoxin detection.

The detection surface was functionalised through ethanol (C_2H_6O) washing, followed by drying in argon. An auto-assembled monolayer (SAM), obtained through the incubation of a thiolic solution of the 11-Mercaptoundecanoic acid for 24 hours, was deposited on the cleansed Au surface. The antibodies were covalently immobilised on the SAM surface, functionalised by means of a N-

Hydroxysuccinimide (NHS)/1-Ethyl-3-(3-dimethylaminopropyl) carbodiimide (EDC). The remaining active areas (on the detection surface) were blocked using ethanolamine.

The first measurements (at constant temperature - 23ºC) were performed with the assembled cell, without the liquid samples. The recorded transfer characteristics will represent the reference values for the phase and amplitude. Constant quantities of liquid were introduced in the sensor's cell and the complex characteristics sets were saved in Touchstone® format for subsequent processing.

The phase shift Δφ of the transfer function is considered to be the most appropriate parameter for the proper read-out of the probe's effect on the sensitive film, because the S_{21} transfer parameter module depends nu just on the acoustic wave propagation conditions, but also on the charge impedance values on the two ports.

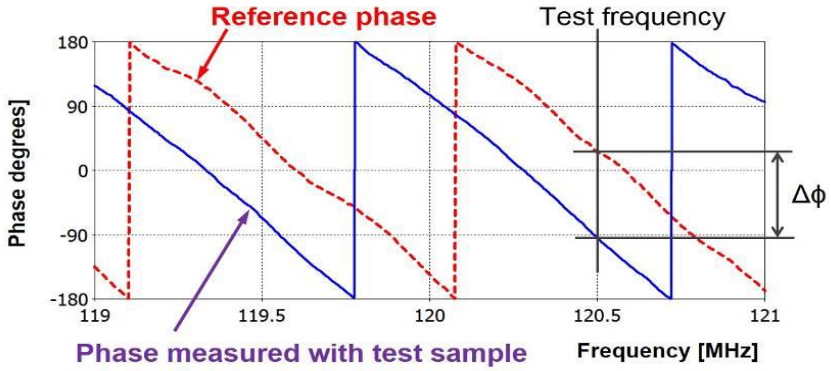

Fig. 3.11 *Measurement of the transfer function phase shift [8]*

The Δφ phase shift, according to Fig. 3.11, is determined at a selected frequency (120.5 MHz) by reading the phase values at the intersection of the line corresponding to the phase shift reading frequency with the two-phase characteristics.

Using this method for a constant frequency (120.4 MHz), a set of measurements for different solution's concentrations was developed. Therefore, the phase characteristics of the transfer function were obtained (Fig. 3.12). The phase variation changes with the solution's concentration increase.

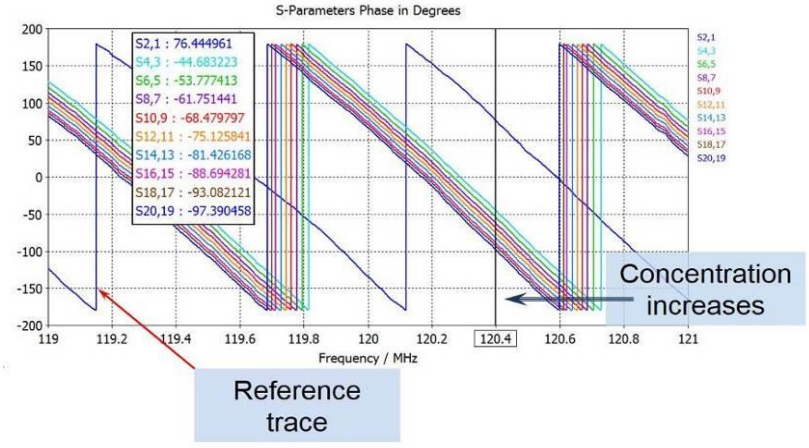

Fig. 3.12 *The phase shift vs. the solution's concentration [8]*

The SAW sensor's response to the immuno-interactions between the liquid sample and its specific antibody shows the dependence towards the mycotoxin concentration (presented in Fig. 3.13). A phase shift increase can be seen for concentrations in the 3-200 nM range.

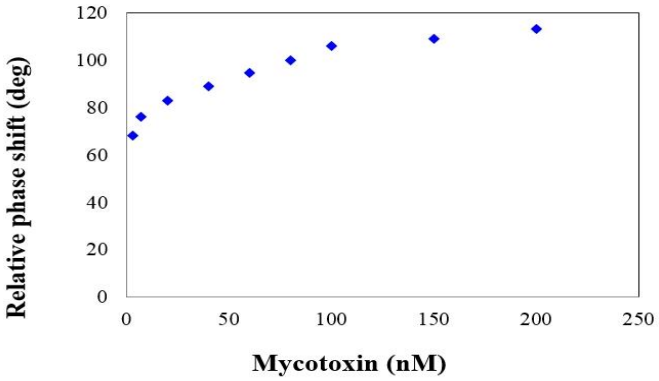

Fig. 3.13 *Modification of the phase shift vs. the mycotoxin solution concentration (120.4 MHz)*

This projection of the phase shift as a function of the mycotoxin concentration solution represents the calibration curve for the chemical sensor. The mycotoxin concentration value in the sample can, therefore, be extracted using this chart, by measuring the phase characteristic of the transfer function. Starting from the transfer function phase value (as measured at 120.4 MHz), found on the chart's ordinate, one needs to draw a line parallel with the Ox axis, that will intersect the calibration curve. The mycotoxin quantity within the sample is the value on the Ox axis, corresponding to the intersection point.

The sensitivity of a sensor is theoretically defined as the variation of its response as a function of the stimulus variation. The SAW chemical sensor sensitivity can be determined from the chart of the phase shift vs. the mycotoxin solution concentration, in the 3-200 nM range. This variation can be linearly approximated on a relatively large range. The obtained sensitivity is S = 0.228 °/nM.

CHAPTER 4

EXPERIMENTAL FABRICATION OF MEMS DEVICES WITH APPLICATIONS TO SENSORS AND MICROWAVES

4.1 Electro-thermal actuators

Electro-thermal actuators are compact and stable devices that need low voltages for actuation. Despite their small dimensions, large displacements may be obtained by mechanical amplification using specially designed configurations [16].

4.1.1 The structure of the electro-thermal actuator

Using low operating voltage, the chevron thermal actuators produce high output forces. The output force (displacement) depends on the inclination angle (α) and the length of the beams (L), Fig. 4.1. When the command voltage is applied on the two pads, electrical current will flow along each pair of arms and the Joule effect will heat them. The resulting thermal expansion of the arms will produce the vertical displacement of the central beam, see Fig. 4.1. The deflection of the Chevron actuator is given by the in-plane shuttle movement and can be expressed as follows [17]:

$$Def_{chev} = [L^2 + 2L(\Delta L) - L\cos^2(\alpha)]^{1/2} - L\sin(\alpha) \quad (4.1)$$

where L is the length of the beam, α is the inclination angle and ΔL is the elongation of the beam due to thermal field.

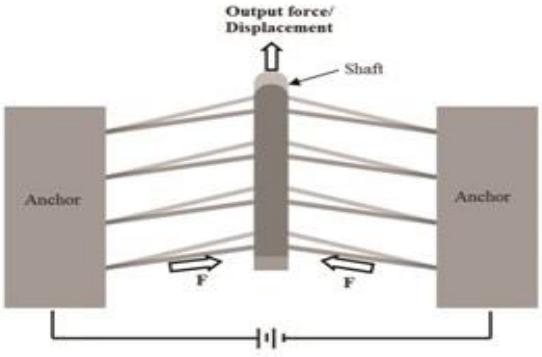

Fig. 4.1 The configuration of chevron actuator

The design of the actuator is shown in Fig. 4.2 with the following dimensions: width of the actuating arms w=10μm, length of the actuating arms L=265μm, spacing between successive arms d=95 μm, number of pairs of arms n=4/5 and the slope angle α=10°.

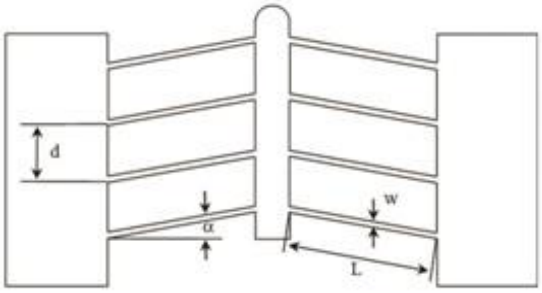

(a)

Fig. 4.2 *Configuration of the chevron-type electro-thermal actuator: Geometry of the device; [18]*

4.1.2 The design of the photolithography masks

We have used for the fabrication of the electro-thermal actuator a single photolithography mask (Fig. 4.3) transferred on the metallic layer. After lithography, the patterned metallic structure is used as a mask for the dry etching of the silicon substrate in order to release the moving parts of the device.

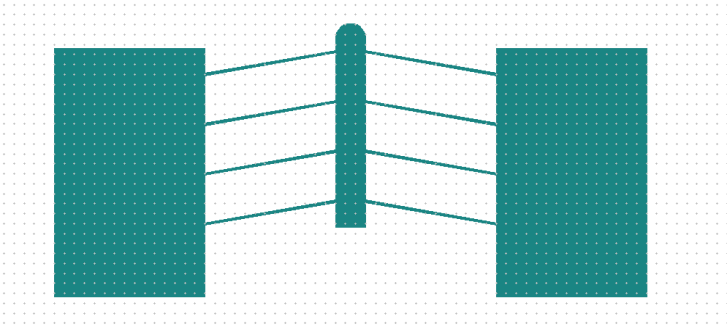

Fig. 4.3 *Photolithography mask used for the fabrication of the electro-thermal actuator*

4.1.3 Development of the technological processes

We used chemical cleaning with "piranha" solution at 110°C to eliminate organic contaminants and other potential impurities from the surface of the silicon wafers. The metallic layer having a thickness of 1μm was deposited directly on the silicon wafer by evaporation (Fig. 4.4 a). The desired pattern was transferred by photolithography on the silicon wafer with metallic layer (Fig. 4.4 b). The Al layer was wet etched in order to obtain the desired pattern (Fig. 4.4 c). The moving parts of the actuator were released by dry isotropic RIE etching of the substrate (Fig. 4.4 e). The technological process is summarized in Fig. 4.4.

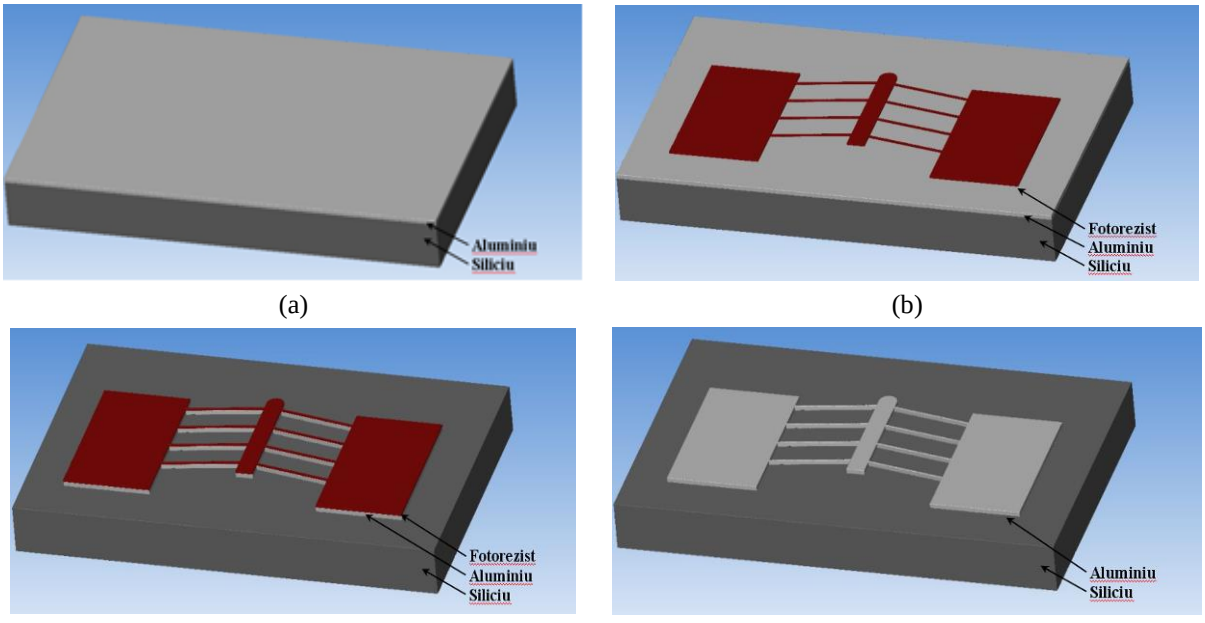

(a) (b)

(c) (d)

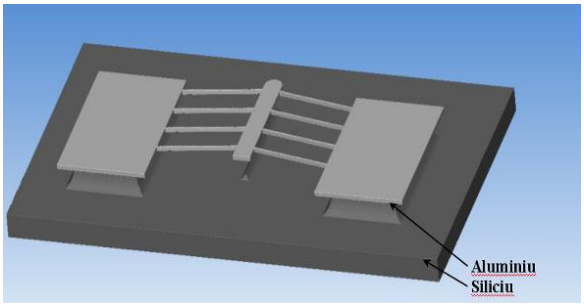

(e)

Fig. 4.4 *The technological process for the chevron-type electro-thermal actuator: (a) Deposition of the Al metallic layer; (b) Photolithography (photoresist spin-coating, exposure and development); (c) Wet etching of the Al metallic layer; (d) Photoresist removal; (e) Dry isotropic etching of the silicon*

During the dry etching process, the pressure was held at 30 Pa (225 mTorr) while the RF power was 200 W for a SF_6 gas flow of 100 sccm. The etch rate was 800 nm/min with approximatively equal values in the vertical and horizontal directions.

This relatively simple technological process has the advantage of good reproducibility of the final structure.

4.1.4 Morphological characterization

We observed the fabricated structures by optical microscopy (Fig. 4.5). The most important parameters are the width and length of the arms and the slope angle.

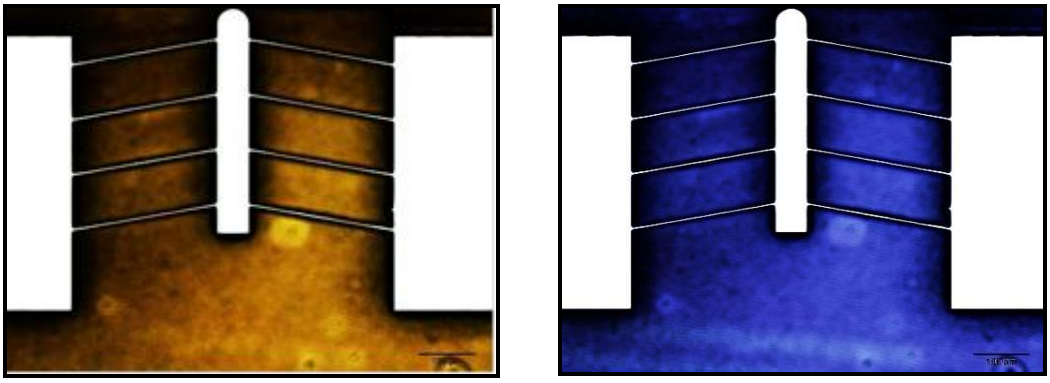

(a) (b)

Fig. 4.5 *Microstructural characterization by optical microscopy: (a) Incandescent lamp; (b) UV lamp [18]*

We note that the simple process we have chosen prevents the large deviation of the slope angle from the design value which appears typically in the wet etching process (Fig. 4.6).

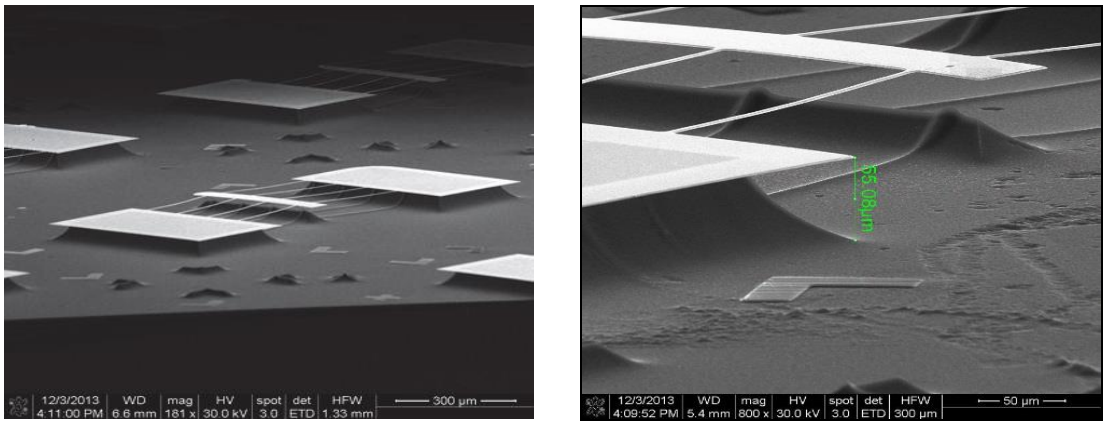

Fig. 4.6 *Microstructural characterization by scanning electron microscopy (SEM)[18]*

The SEM images in Fig. 4.6 show the complete release of the central beam with a etch depth of approximatively 55μm depth after the release of the moving part.

4.1.5 Electrical characterization

The voltage applied to the device pads was in the range 0.05-0.2V, with resulting currents in the range 93-250 mA. Fig. 4.7 shows an optical image of the device during electrical measurements, with the two probes positioned on the pads clearly visible.

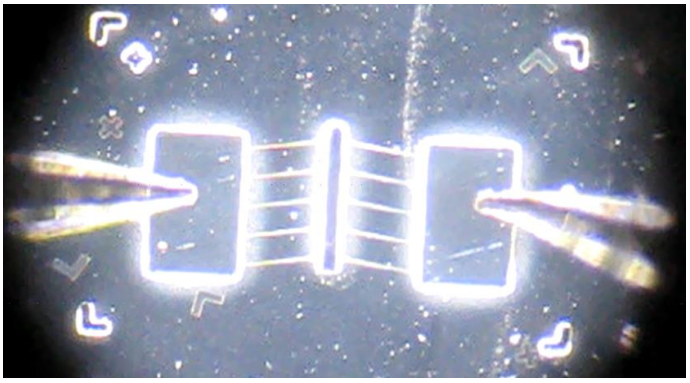

Fig. 4.7 *Optical microscope image of the device during electrical measurements*

The measurements show that the maximal displacement of the central beam is around 12 μm for an applied voltage of 0.2 V and a current of 250 mA. We note that the vertical displacement of the central beam depends on slope angle and applied voltage.

4.2 RF-MEMS switches with electro-thermal actuation

RF-MEMS switches are better candidates compared to conventional switching devices based on FET transistors (Field Effect Transistor) or PIN (P-type / Intrinsic / N-type) diodes [19]. RF-MEMS switches with electro-thermal actuation are constituted by a controlled contact via actuators. In this case, the contact is connected in series with the line on which the signal propagates, eliminating the interdiction of the continuous voltage transmission through the coplanar line signal conductor. Although the reaction speed of the thermal actuators is smaller due to deformation processes, the thermal actuation system is more robust from the mechanical point of view and does not require the introduction of dedicated structures to return the switch to the stable equilibrium position.

4.2.1 The design of the RF-MEMS switches

To reduce the complexity of the RF-MEMS design, mainly due to the requirements of both a large frequency band from DC up to several GHz and a mechanical structure showing controllability and stability, we have split the device in two subsystems (Fig. 4.18): (i) the set of two thermal actuators used for actuation and (ii) the coplanar waveguide (CPW), which ensures the operation of the switch function in a large frequency band.

The working principle of the RF-MEMS switch is simple: the actuation of the system containing the symmetrically positioned electro-thermal actuators heats and expands the central part of the switch (polymeric structure) by Joule effect and thermal expansion. The chevron-type arms connecting the two actuators push the central part of the switch toward the CPW lines until contact is made (ON position). By changing the electrical actuation from the outer arms to the inner ones, the central part is pulled back to the OFF position of the RF-MEMS switch.

The test configuration of the RF-MEMS is presented in Fig. 4.8. This design is relatively simple in comparison with the typical bistable actuation design usually found in the literature and can be used a test structure to check both the technological process and the electrical and thermal behaviour.

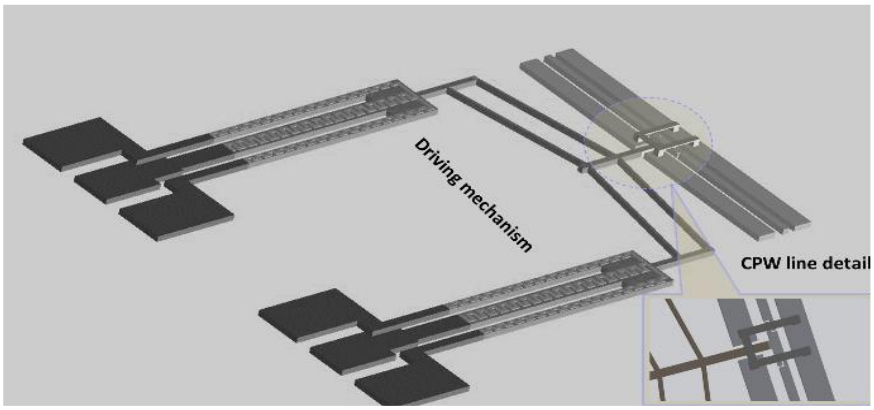

Fig. 4.8 *Test configuration of the RF-MEMS switch [20]*

4.2.2 The design of the photolithography masks

The actual fabrication of the RF-MEMS switch has been realized with three photolithography masks. The design stage was done with the software CleWin and corresponds to the main following steps:

- *Patterning the first SU-8 polymer layer using photomask **M1**;*
- *Deposition of metallic films (Cr/Au–200 nm) and patterning using photomask **M2**;*
- *Patterning of the second SU-8 polymer layer using photomask **M3**;*

The actuation structure is a sandwich of two polymeric SU-8 layers with the electrical heating element (Cr/Au) embedded between them. The microwave system is made of Cr/Au but for the test structure it was taken as a simple electrical contact (Fig. 4.10).

The first photolithography mask was designed such that it provides the actuation mechanism made of SU-8. Fig. 4.9 shows this first mask; one can easily observe on the same figure the two electro-thermal actuators and the central beam that makes or breaks the electrical contact. The central beam was patterned with an array of quadratic holes of 20 x 20 μm to permit an easy access of the etching solution to the sacrificial layer and the rapid release of the final structure. This mask takes into account the fact that the SU-8 polymer is a negative photoresist.

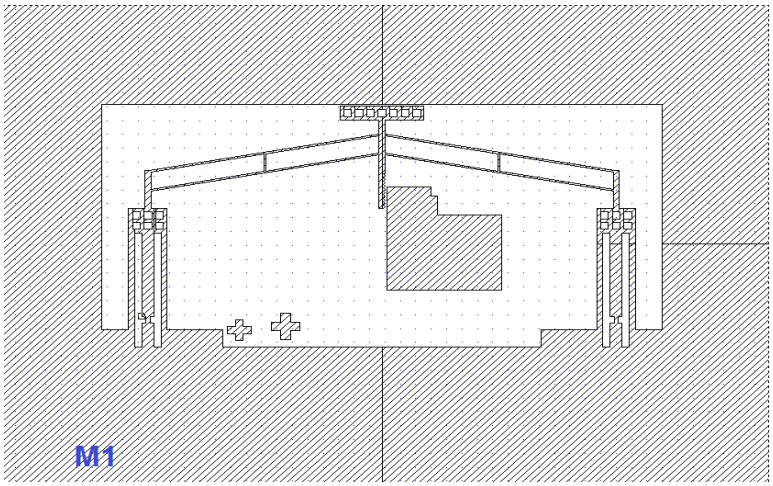

Fig. 4.9 *The first photolithography mask used to pattern the actuation mechanism*

The second photomask, shown in Fig. 4.10 , is used to define both the metallic resistor used as heater for the actuation mechanism and the CPW lines. The first test will be done on the simple structure where the electrical contact part is simplified and contains only the central beam. The electrical heater is defined in the photomask M2, has a meander form on the hot (lateral) arms and forms a continuous

film on the cold (central) arms. The width of the meander has been taken as 5 μm. Note that the heater meander follows the form of the cold arms with a narrow region which promotes the arching and the movement of the beams during electro-thermal actuation.

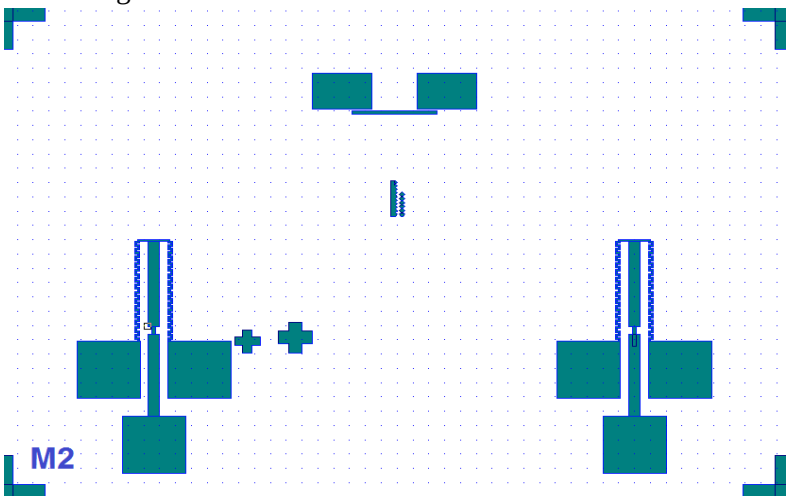

Fig. 4.10 *The second photolithography mask used to pattern the metallic heater film and the CPW lines*

We have also included in the central part of the chip a calliper that permits the live optical measurement of the vertical displacements of the final structure during actuation with a precision better than 1μm.

The third and last photomask (Fig. 4.11) is used to pattern the second polymeric layer that assures the symmetric embedding of the metallic heater and therefore prevents the out-of-plane displacements of the switch.

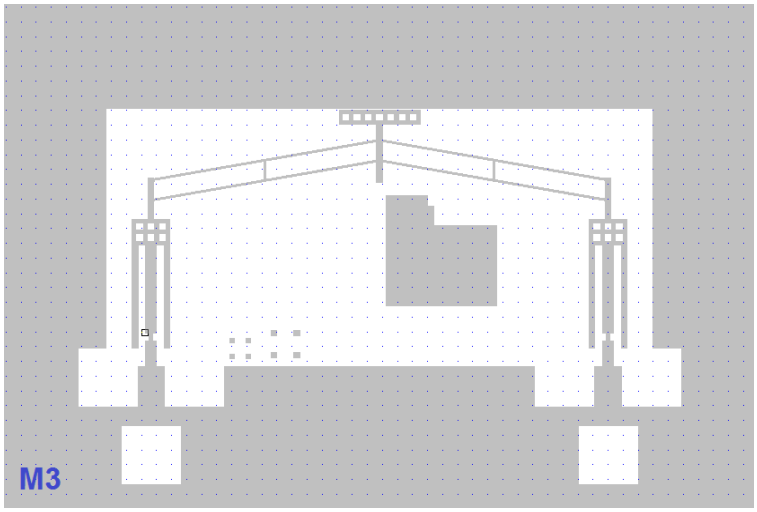

Fig. 4.11 *The third photolithography mask used to pattern the actuation mechanism*

A final view of the three, superposed photomasks used for the fabrication of the actuation mechanism is shown in Fig. 4.12. We note the inclusion of several alignment marks that take into account the polarization of each mask (positive or negative).

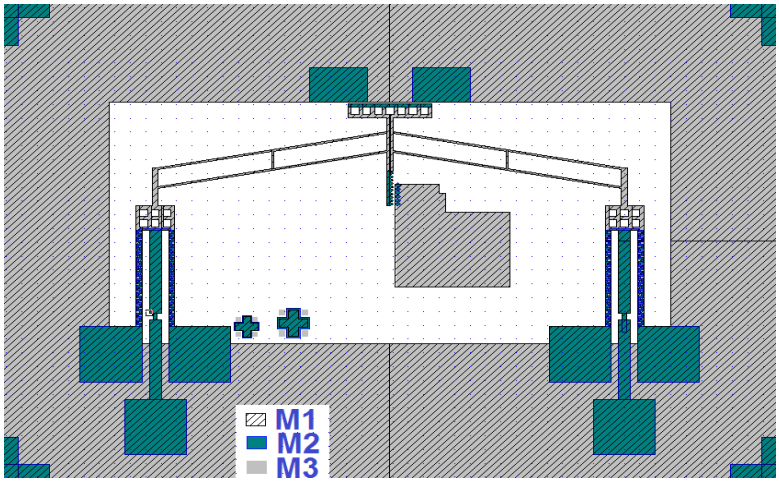

Fig. 4.12 *The superposition of the three masks used for the fabrication of the RF-MEMS switch*

4.2.3 Description of the technological processes

Fig. 4.13 shows the diagram of the technological process needed to obtain the RF-MEMS switch. The first step is the cleaning of the Si wafer in "piranha" solution, followed by cleansing in deionized water (DI).

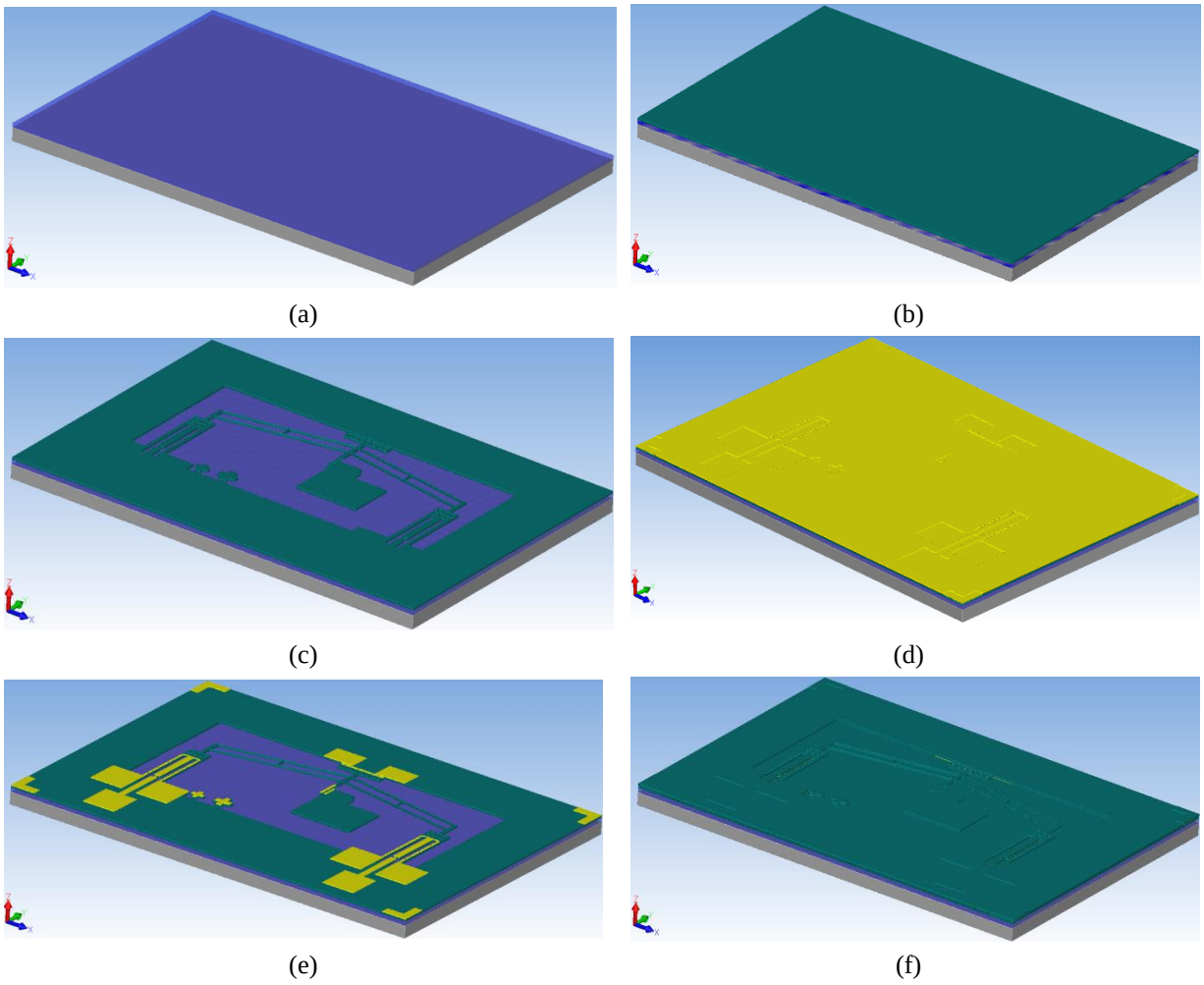

(a) (b)

(c) (d)

(e) (f)

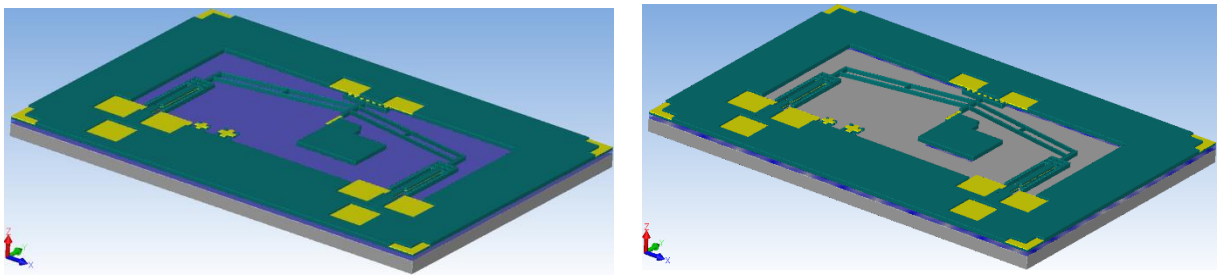

(g) (h)

Fig. 4.13 *The technological process for RF-MEMS switch: (a) Thermal oxidation of the silicon wafer; (b) Deposition of the first layer of SU-8; (c) Patterning of the first SU-8 layer using photomask M1; (d) Deposition of the metallic layer Cr/Au; (e) Patterning of the metallic heater and CPW lines using photomask M2; (f) Deposition of the second SU-8 layer; (g) Patterning of the second SU-8 layer using photomask M3; (h) Release of the structure by etching the sacrificial SiO_2 layer*

In order to obtain a silicon dioxide film with thickness of 1.7μm to be used later as sacrificial layer, we thermally oxidized the silicon wafer (Fig. 4.13 (a)). Next step consists in the deposition by spin-coating of the SU-8 layer with a thickness of 5μm. The patterning of this layer was done by developing the polymer using the photomask M1 (Fig. 4.13 (b) and (c)). Next, the metallic Cr/Au layer with a thickness of 200 nm was deposited by evaporation, patterned by photomask M2 and lift-off (Fig. 4.13 (d) and (e)). The second layer of SU-8 with a thickness of 5 μm was deposited by spin-coating (Fig. 4.13 (f)) and patterned using the last photomask M3 (Fig. 4.13 (g)), so that the thermal heater was sandwiched between two polymeric layers having equal thicknesses. This layout not only isolates electrically the metallic layer, but also eliminates the out-of-plane movements of the switch due to thermal mismatch between the polymeric and metallic layers. The last step consists in the isotropic etching of the sacrificial layer in order to release the moving structure (Fig. 4.13 (h)).

For the release of the structures we tested two different methods for etching the sacrificial SiO_2 layer: in HF vapors and wet etching. Best results were obtained with the HF vapor etching which significantly reduces the risk of the released structure sticking to the substrate. The HF vapor etching was done at 37°C with an etching rate of 430 nm/min. The wet etching was done in BHF solution at 23°C with an etching rate of 100 nm/min.

4.2.4 Morphological characterization

The optical characterization of the structures was done after each process step. Fig. 4.14 (a) shows a detailed view of the beam representing the moving contact for the CPW lines. Another critical step was the patterning of the metallic heater and the CPW lines, with an optical view shown in Fig. 4.14 (b).

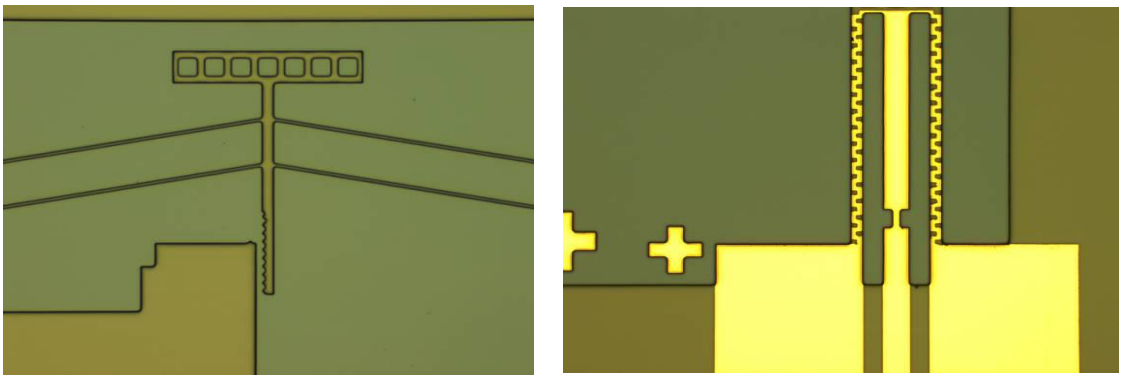

(a) (b)

Fig. 4.14 *Optical view of the structure after patterning the first SU-8 layer: (a) The region of the contact beam; (b) detailed view of the patterning of the heater*

At the end of the technological process we did a SEM characterization of the final devices (Fig. 4.15), including a detailed investigation of the surface obtained by vapour etching.

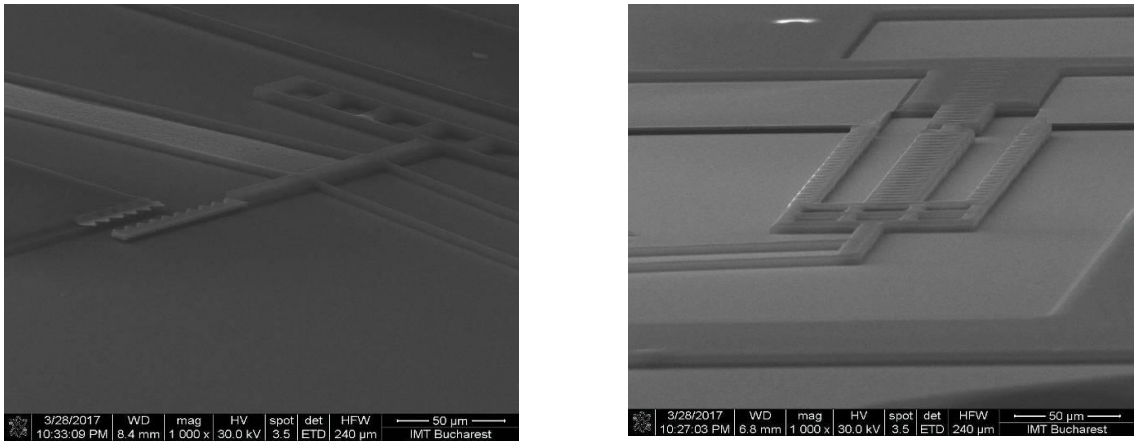

(a) (b)

Fig. 4.15 *SEM images of the fabricated RF-MEMS: (a) Metallic contact; (b) Electro-thermal actuator, part of the actuation mechanism*

Fig. 4.15 (b) shows that this surface is clean without any additional compounds formed by chemical reaction of the hydrofluoric acid with the SU-8 polymer.

The next stages are the electrical and RF testing of the obtained devices using a vector network analyzer. (VNA).

4.3 Technology of cantilever fabrication

Electrostatically actuated cantilevers have been used for vibration sensing. In this section we mainly pursued techonological steps and tribological characterization of structured materials that bring significant enhancement of electrostatic behavior of fabricated devices. Thus deposition conditions of polysilicon films were varied and tuned in order to obtain optimal material parameters for the given application.

4.3.1 Cantilever configuration

The cantilever consists of a beam clamped at one end and free at the other end and an actuating electrode (the bottom electrode), between which the drive voltage U is applied. The main design parameters of the device are: t_p *– cantilever thickness, L – cantilever length, w – cantilever width,* g_0 *– a gap which is the thickness of the sacrificila layer,* t_p *– the ticknes of the bottom (actuating) electrode (*Fig. 4.16).

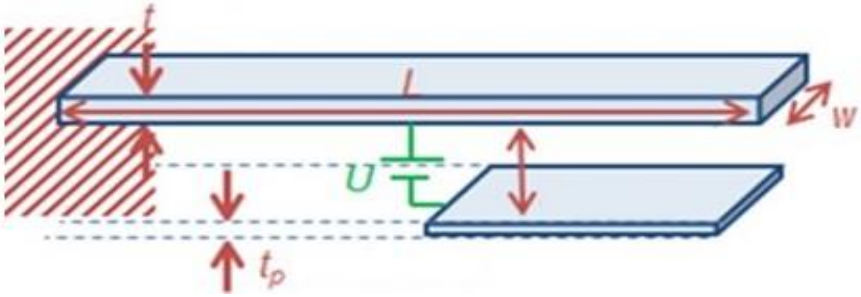

Fig. 4.16 *Design parameters of cantilever[21]*

4.3.2 Design of the photolithography masks

There were used three photolithography masks for cantilever fabrication. The design step has been performed by using CleWin software according to the following technological flux:

- *Patterning of n doped polysilicon using the mask **M1**;*
- *Patterning of sacrificial layer using **M2** mask;*
- *Patterning of n doped polysilicon second layer using the mask **M3** – cantilever fabrication;*

The first photolithography mask was used for pattering the n doped polysilicon to obtain the actuating electrode. The mask is presented in Fig. 4.17.

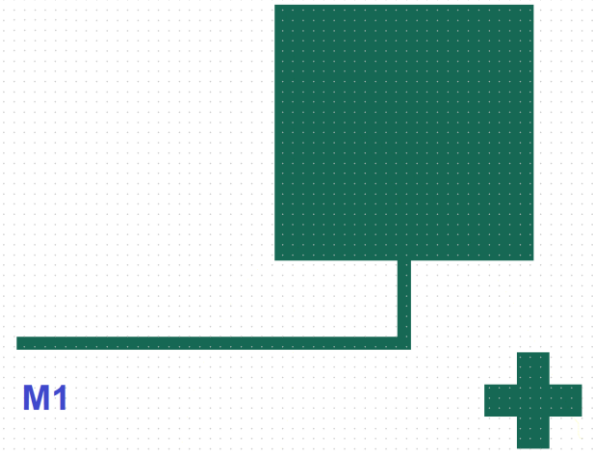

***Fig. 4.17** The photolithography mask for pattering the actuating electrode (M1);*

The next technological step is the deposition of sacrificial layer and implicitly its patterning. Thus, the second mask has the role of window opening in the SiO_2 layer in the pad area for facilitating the deposition of the next polysilicon layer. The configuration of the second photolithography mask is illustrated in Fig. 4.18.

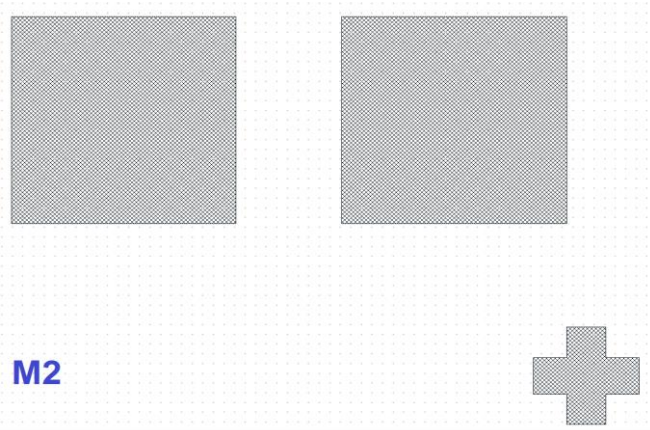

***Fig. 4.18** The second mask (M2) for opening of windows in the SiO_2 layer;*

According to Fig. 4.18 after the etching process there are obtained two windows in the sacrificial layer where the last polysilicon layer is deposited.

The role of the next mask is to define the cantilever and the pads. The mask has various versions with different sizes of cantilever length and width, while the pads have the size of 400 μm × 400 μm. Fig. 4.19 shows the last mask.

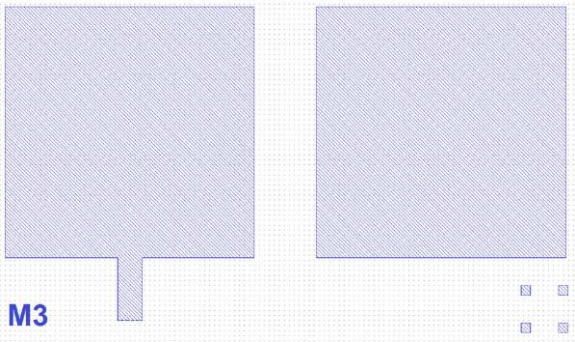

Fig. 4.19 *Photolithography mask for cantilevel patterining (M3)*

This photolithography mask has been designed and fabricated for positive photoresist protects the interest areas on wafer. Following the etching of the last n-doped polysilicon the cantilevers will be well defined on wafer. A view of all there aligned masks on wafer is provided in Fig. 4.20.

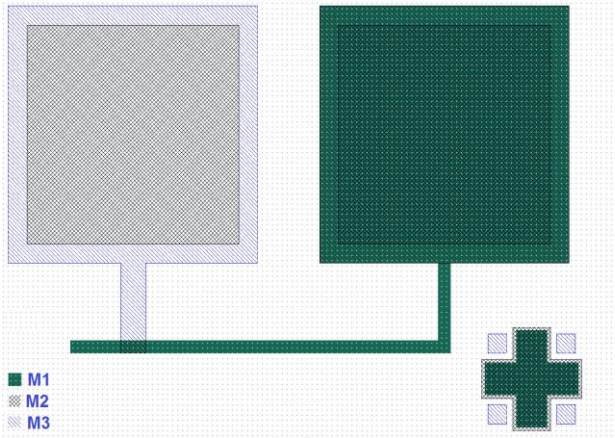

Fig. 4.20 *The superposition of the three masks used for the fabrication of cantilever structures*

On the wafer for device testing we opted for several cantilever structures seen in Fig. 4.21, where there are 32 cantilevers of various sizes.

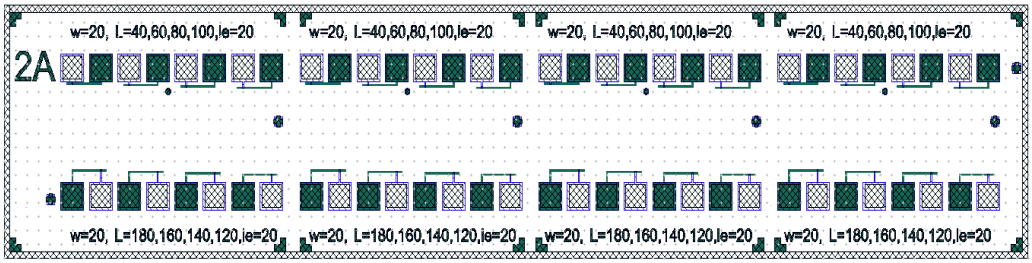

Fig. 4.21 *On chip configuration of cantilever structures*

4.3.3 Description of technological flux

To remove the organic residues on the wafer it was used an acid-based solution called „piranha". The next step it the removal of unwanted native oxide off the wafer in an acid solution of HF diluted in water. On the cleaned wafer by LPCVD technique we deposit a film of 300 nm thickness silicon nitrite. Si_3N_4 was obtained as a reaction product of dichlorosilane (H_2SiCl_2) and ammonia (NH3) at 780ºC. The role of Si_3N_4 is to insulate the devices from the substrate. The Si_3N_4 deposition is followed by the deposition of thin film of polysilicon by the same method of low pressure CVD (PLCVD). The major advantage of the method consists in uniformity, homogeneity and reproducibility of films.

The polysilicon films are obtained from the pyrolysis of silane (SiH_4) at temperatures between 550ºC and 675ºC. The properties of thin films obtained by LPCVD are determined by the pressure and concentration of silane as well as by the temperature. Accordingly, a special care was considered for

determining optimal parameters of polysilicon deposition to fabricate successful cantilevers. Thus, the polysilicon thickness was 2 μm at four temperatures, 580ºC, 610ºC, 630ºC and 650ºC, and 0.2 mbar pressure. In Fig. 4.21, from SEM images one can see the roughness of the films.

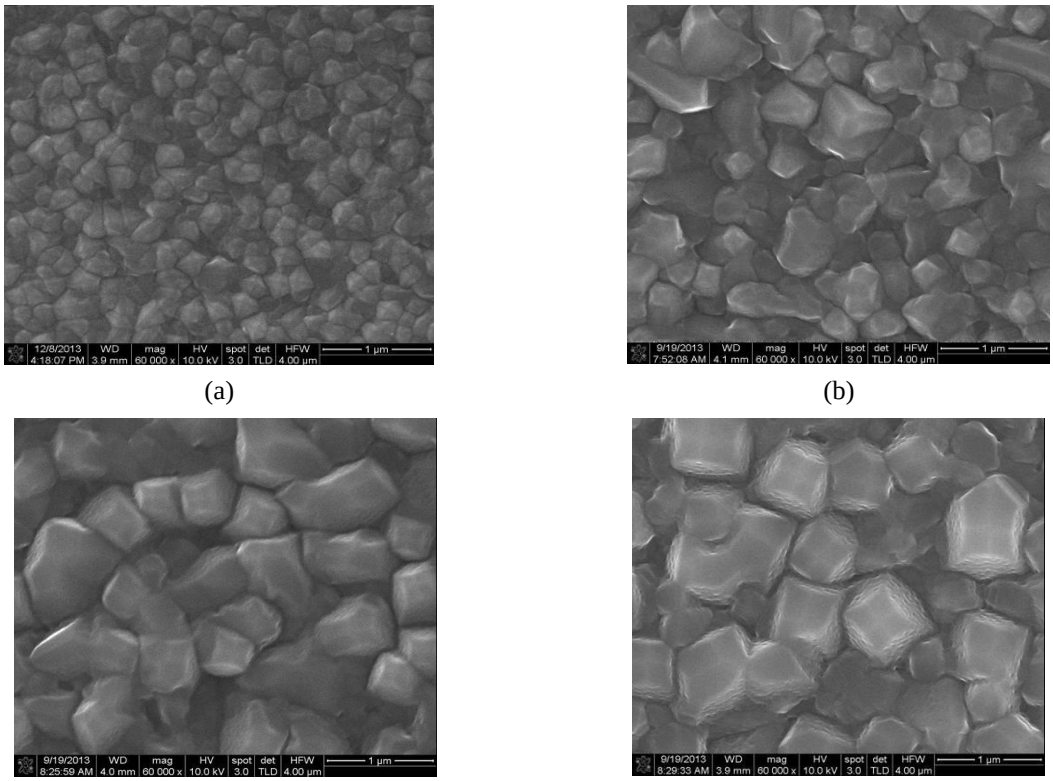

(a) (b)

(c) (d)

Fig. 4.22 *SEM images of various polysilicon samples deposited at: (a) 580ºC; (b) 610ºC; (c) 630ºC and (d) 650ºC [22]*

One can notice that by increasing the growth temperature the roughness changed, and the size of grains increased. The surface morphology of polysilicon was also characterized with AFM (Atomic Force Microscope) and was shown in Fig. Fig. 4.23.

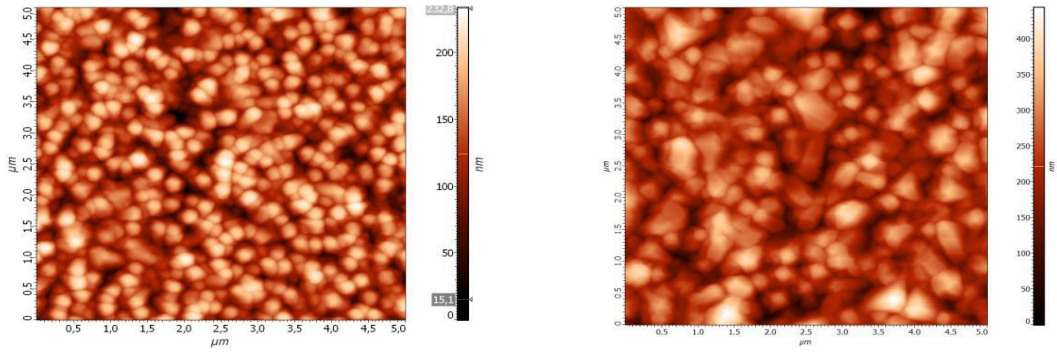

(a) (b)

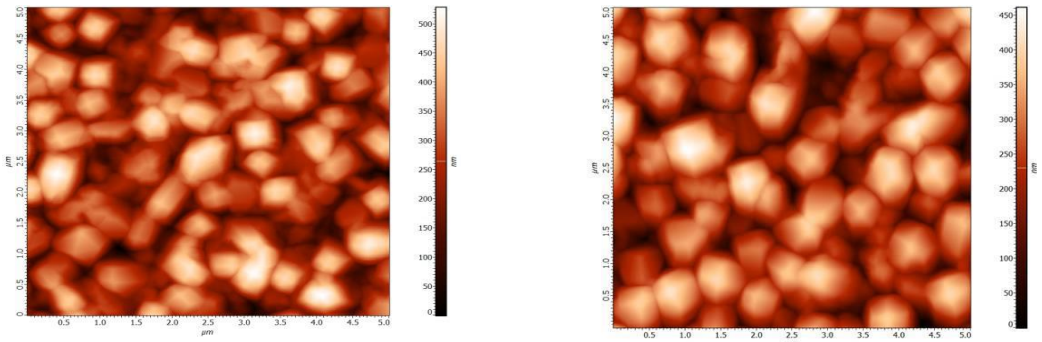

(c) (d)

Fig. 4.23 *AFM images of of various polysilicon samples deposited at: (a) 580ºC; (b) 610ºC; (c) 630ºC and (d) 650ºC [22]*

The average sizes of grains for films grown at T=580ºC are about 190 nm, while those of films grown at T=650ºC range from 750 to 800 nm.

Using the X-ray diffractometry technique (XRD) it was studied the degree of film crystallinity. Thus, for polysilicon deposed at T=580ºC it was measured a degree of cristallinity of 97.48 %, while for higher temperatures the cristallinity reached 100 %. To improve the cristallinity of films obtained at 580ºC thermal treatments in N_2 atmosphere were performed at 900ºC for 30 minutes.

To fully characterize the film, it was also determined the Young modulus with a Berkovich indenter of 20 nm radius belonging to G200 Nanoindenter module from Agilent Technologies. The average measured values of Young modulus are presented in Fig. 4.24.

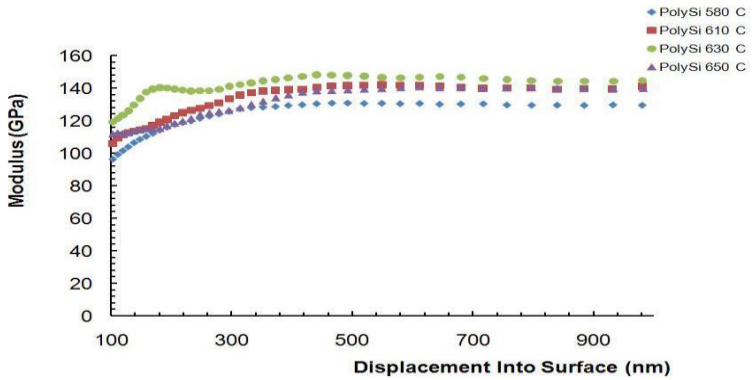

Fig. 4.24 *Young modulus as a function of tip penetration depth for polysilicon samples grown by LPCVD at: 580ºC, 610ºC, 630ºC şi 650ºC [22]*

The average value of Young modulus was about 140 GPa for all grown polysilicon samples except that grown at 580ºC which was 130 GPa.

The polysilicon doping was performed in a diffusion furnace at 1000ºC for 30 min using a source of phosphorus (P). In Fig. 4.25 one can see the AFM profiles of polysilicon samples after diffusion process.

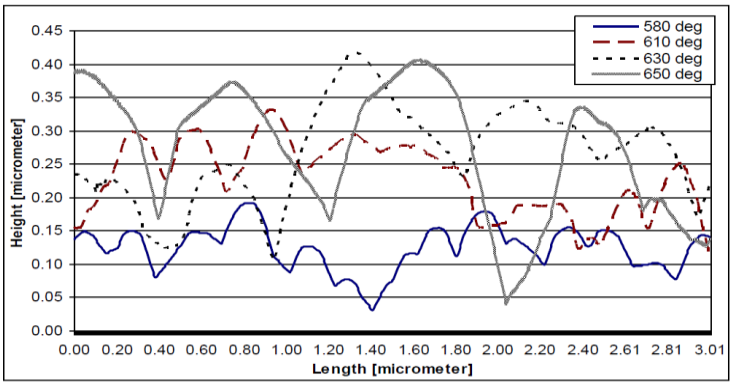

Fig. 4.25 *AFM al eşantioanelor de polisiliciu după procesul de difuzie cu fosfor[22]*

After doping it was observed a significant decrease of surface roughness. The smallest value was obtained for samples grown at 580 ºC. The average roughness value for undoped polysilicon was Sq = 35.55 nm, while for doped polysilicon was just Sq = 25.71 nm. Based on the above values of roughness and Young modulus the temperature of 580ºC was chosen for film growth of polysilicon. This temperature ensures the optimal roughness and Young modulus for cantilever fabrication.

With the first photolithography mask (**M1**) and using anisotropic dry etching by RIE it was patterned the bottom electrode made of doped polysilicon with a thickness of 150 nm (Fig. 4.26 (a)). Optical image of bottom electrode can be seen in Fig. 4.27 (a).

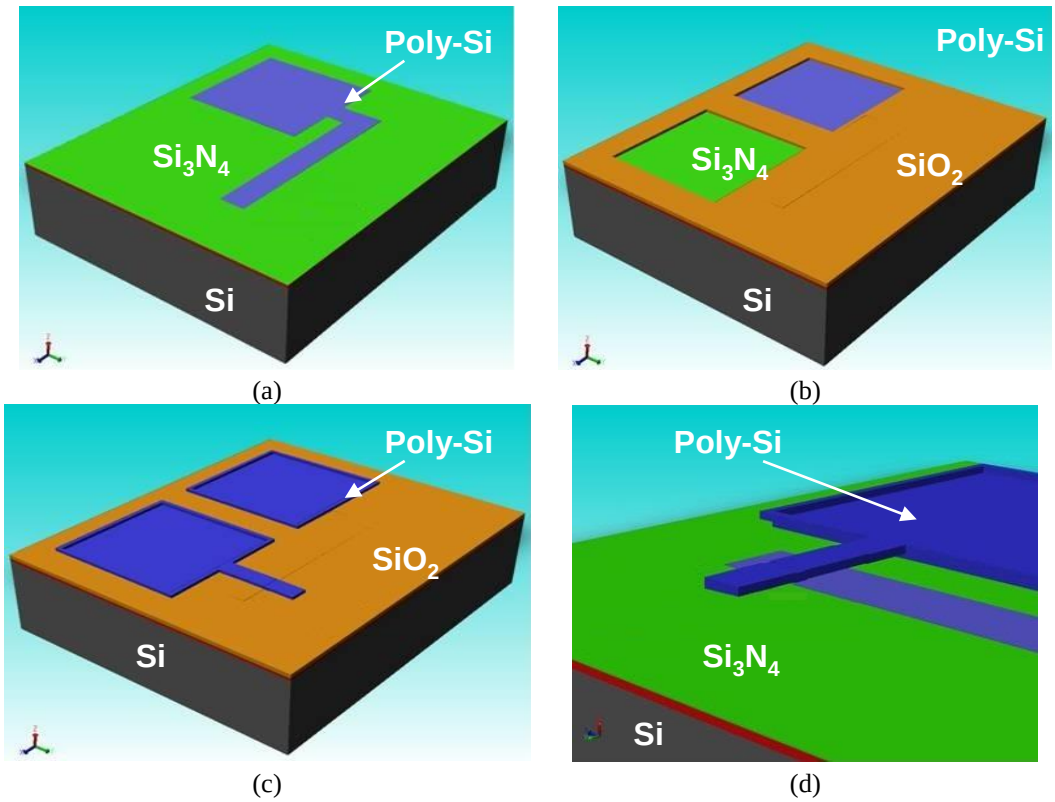

Fig. 4.26 *Schematics of the technological flux to obtain polysilicon cantilevers: (a) Patterning of the bottom electrode with the help of mask M1; (b) Window opening in the sacrificial layer using mask M2; (c) Patterning of cantilevers fabricated of polysilicon with a 2 µm thickness using mask M3; (d) Cantilever release by wet etching of sacrificial layer.*

The next technological step was the deposition by PECVD of the sacrificial layer of SiO_2 having a thickness of 2 µm. The patterning of silicon dioxide was done with mask **M2** by wet etching with a

solution of BHF (schematic shown in Fig. 4.26 (b)). In Fig. 4.27 (b) we present the optical image of the electrode (on wafer).

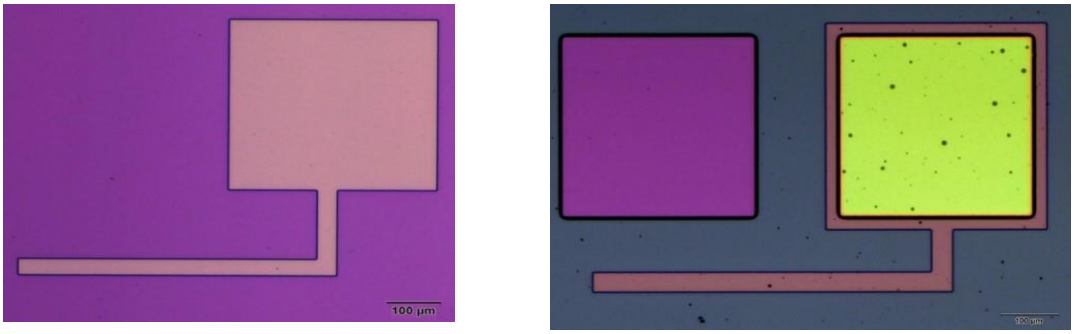

(a) (b)

Fig. 4.27 *Optical image of Si wafer :(a) After bottom electrode patterning in polysilicon and (b) after window opening in sacrificial layer.*

To obtain the cantilevers a new polysilicon layer of 2 µm thickness was deposited. The n-doping of polysilicon was performed in the same diffusion furnace using a P source at 1000ºC for 30 min. The plane resistance of the sample was measured and a value of 4,4 Ω/□ was obtained. Using the last mask (**M3**), the cantilevers were obtained through anisotropic dry etching of polysilicon by RIE (Fig. 4.26 (c)). The optical image of the obtained device can be seen in Fig. 4.28.

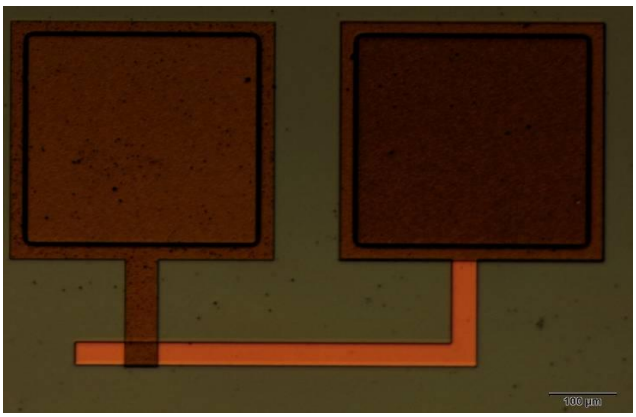

Fig. 4.28 *The optical image of the obtained devices*

The last technological step was the release of the microstructures by wet etching of sacrificial layer in hydrofluoric acid (HF) (Fig. Fig. 4.29).

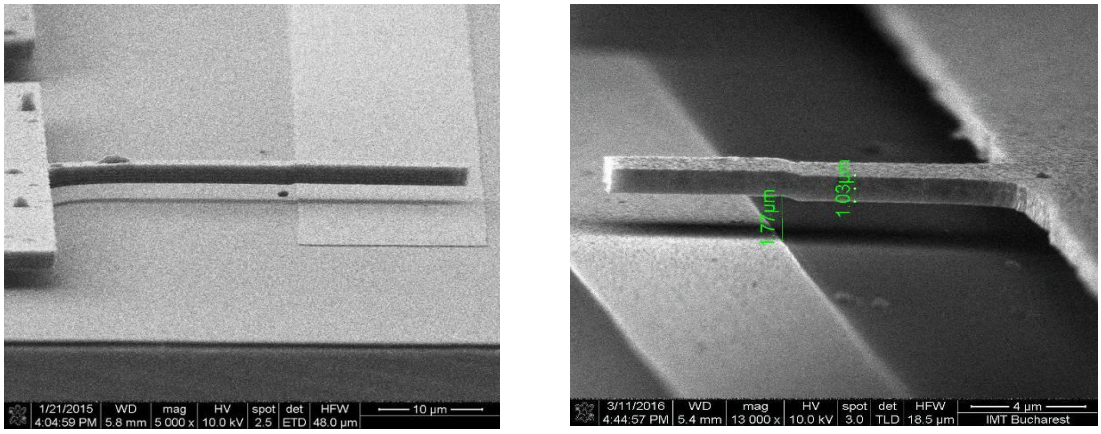

Fig. 4.29 *SEM pictures of cantilevers obtained by surface microfabrication [21]*

4.3.4 Electrostatic characterization

Electrostatic characterization of cantilevers was performed with the tester Keithley 4200-SCS for wafer characterization. The electric behavior was analyzed from I-V curves. To observe the actuating voltage a measurement setup was made whose results were given in Fig. 4.30. To determine the operating voltage of the cantilevers the starting ***applied voltage was 0 V.*** The ***actuating voltage increased in 0,5 V steps until 210 V*** and it *was established a value of the* ***limiting current to 105 µA.***
In Fig. 4.30 it can be seen that, for a structure with w=10 µm and L= 45 µm, the actuating voltage is 205 V which corresponds to a jump of the current to higher limiting value of 105 µA. For a cantilever having a twofold increase of its width and the same length the actuating voltage drops to 110 V for a limiting current of 105 µA. After actuation the voltage drops to 0 V and the cantilever sticks to the bottom electrode.

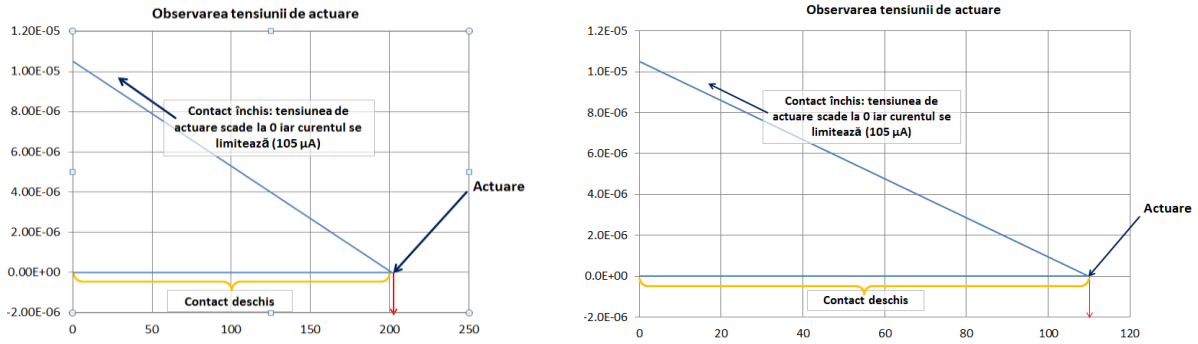

(a) (b)

Fig. 4.30 *Measuring the actuating voltage for two types of cantilevers: (a) w = 10 µm, L = 45 µm and le = 20 µm;(b) w = 20 µm, L = 45 µm and le = 20 µm*

The I-V characteristics presented in Fig. 4.30 show the actuating voltage of the cantilevers varies inverse proportionally with their width.

CHAPTER 5

TECHNOLOGICAL PROCESSES ON SIC

The research presented in this chapter was focused on the study and optimization of microprossesing of SiC in order to obtain MEMS structures out of this material. The SiC wafers used in these studies were n-doped 4H-polytype SiC of epitaxial 8 μm thickness.

5.1 Preparation of SiC samples

Although SiC is a chemical inert material, for further microprocessing it needs a wet chemical cleaning to remove any impurity that can lay on its surface. The cleaning process may follow several steps:

- In a first stage the wafers were cleaned in organic solvents;
- To remove organic residues from the wafer surface it was used a „piranha" solution made of H_2SO_4 and H_2O_2 in a ratio 3:1;
- A water diluted HF was used to remove the native oxide off the wafer surface;

5.2 Dry oxidation of SiC

Thermal oxidation in O_2 atmosphere (dry) of the first sample was performed at T=1100℃ for 30 minutes. The second process was performed in the same conditions but for an oxidation time twice the one used for the first run. The thickness of the oxide films were measured with the refractometer Nanocal XR in 9 points and the roughness was evaluated by XRD. The results are summarized in the table below:

Tab. 5.1 *Thermal oxidation of SiC samples*

	Measured points									***Non-uniformity***	***Roughness***
Pb.1-time: 30 min	1	2	3	4	5	6	7	8	9	5.30 %	1.99 nm
Thickness (nm)	59.5	58.9	65.5	60.6	60.2	60.5	59.5	59.2	59.4		
Pb.2-time: 60 min	1	2	3	4	5	6	7	8	9	1.71 %	2.04 nm
Thickness (nm)	69.6	68.7	71.1	70.5	70.2	70.9	69.7	69.3	69.5		

By dry oxidation of SiC wafers there were obtained oxide films with various thicknesses: 60 nm for an oxidation time of 30 min and 70 nm for an oxidation time of 60 min. The oxidation speed is very small (half of the oxidation speed of Si). From Tab. 5.1 one can see that the non-uniformity is smaller for thicker films while the roughness remains pretty much the same.

5.3 SiC dry etching by RIE

To avoid the process of micro-masking it was chosen for the mask Nickel silicide to etch 4H-SiC. Nickel silicide is quite resistant for plasma etching. The samples in this study used 700 nm thick films of NiSi with the lift-off technique.

The etching of 4H-SiC was performed in a capacitive reactor-reactive-ion etching (RIE) equipment with a mix of gases (SF_6 and O_2). The oxygen concentration varied about 10 %. This gas along with various roles described in the literature can react with Ni in order to form NiSi. Other possible chemical reaction between O_2 and Ni is that to obtain nickel oxide which is also more resistant than Ni to plasma etching of SiC [23].

The first etching tests were done at a pressure of 20 Pa, a *rf* power of 250 W and a mix of SF_6 and O_2 with fluxes of 100 sccm and of 10 sccm, respectively. The etching time was established for 3 cycles of 5 min each with 2 min between cycles. The role of these breaks was to maintain the substrate temperature low to avoid its influence on the etching process. The first measurements performed at 15 min after the etching with a profiler showed an etching depth of 100 nm that gives an etching rate of 6.6 nm/min which is quite low for a process of MEMS fabrication. The etched surface showed high roughness that indicates a need for improving the etching process by increasing the etching rate and by lowering the surface roughness.

The increase of etching rate can be done first by increasing the gas pressure hence increasing the reactance of plasma. Increasing the pressure allows the increase of the collision rate between the species in plasma, but also it decreases the anisotropy of etching. The second way to increase the etching rate is energy of the ions. This is done by increasing the rf (radiofrequency) power. By this procedure it is increased the concentration of radicals, thus many more ions with high energy will be present leading to lower selectivity.

The rf power as well as the oxygen flux were increased. In Tab. 5.2 one can see the plasma parameters for the most relevant etching processes of SiC.

Tab. 5.2 *The etching parameters of SiC probe (CCP RIE)*

Plasma etching parameters of SiC by RIE (CCP RIE)							
Process	1	2	3	4	5	6	7
Rf power (W)	250	350	350	450	450	250	250
Pressure (Pa)	20	20	30	30	30	10	10
The flow rate of SF_6 (sccm)	100	100	100	100	100	45	15
The flow rate of O_2 (sccm)	10	10	10	10	30	9	6
Number of etching cycles (1 cycles =5 min)	3	3	3	3	3	3	2

* (sccm- Standard Cubic Centimetres per Minute)

5.4 Morphological characterization of the etched surface

To measure the etching depth and to characterize the etched surface the metallic mask was removed in Iron trichloride ($FeCl_3$). As it can be seen in Fig. Fig. 5.1, the etching depth was approximately 827 nm. This depth was obtained by performing 3 etching cycles of 5 min each resulting in an etching rate of 53.15 nm/min in contrast to 6.6 nm/min initially obtained. Thus, the rate increased but the roughness is still very high.

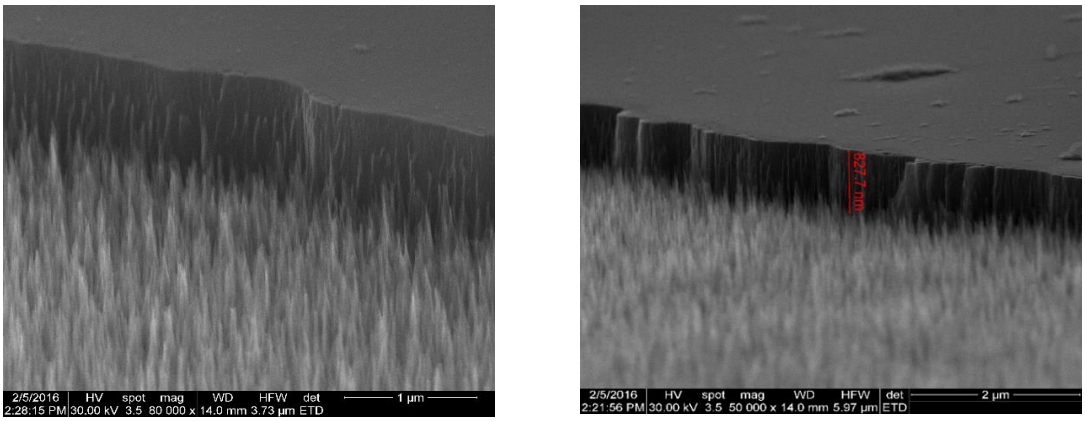

(a) (b)

Fig. 5.1 *SEM image of etched surface using the recipe no. 6 (a) Characterization of etched surface; (b) Measurement of etching depth*

Given the fact that the roughness is high an AFM investigation cannot be done properly. By contact profilometry the measured etching rate was 47.03 nm/min. Therefore, the second goal was to obtain a better roughness. In order to pursue this, gas fluxes were reduced for both SF_6 (to 15 sccm) and O_2 (to 6 sccm). In Fig. 5.2 one can see the roughness was improved by reducing the size as well as of the shape of "grass".

However, the etching depth was smaller due to shorter etching time. Also, the mask was not removed in order to see the low selectivity of mask with respect to etching character of plasma.

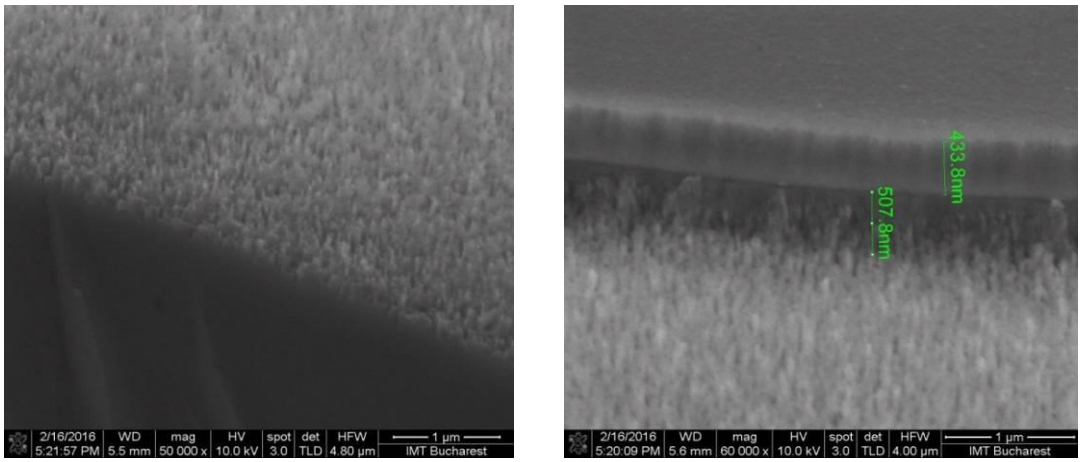

(a) (b)

Fig. 5.2 *SEM image of etched surface usinf the recipe no. 7 (a) Chatracterization of etched surface; (b) Measurement of etching depth*

In Fig. Fig. 5.2 (b) one can notice that a process of 10 min can etch about 265 nm of NiSi mask. In conclusion this recipe can be used for etching thin films of SiC.

CONCLUSIONS

The research presented in this thesis is aimed to provide a comprehensive analysis of different fabrication processes for MEMS sensors and structures and is also dedicated to address new technological solutions in order to improve devices performances. Chemical sensors, together with MEMS devices in the field of microwave and vibration sensors, have been designed and manufactured in order to achieve this purpose. In this respect, there have been investigated fundamental aspects in the development of some reliable and high-performance sensors and MEMS devices, described over the course of five chapters, which have led to the proposed objective.

Taking into account the evolution of MEMS devices market - that is presented in ***Chapter I*** - during this work we have tried to obtain devices with comparable performances with the one already on sale, but being optimized as regarding fabrication costs.

In ***Chapter 2***, titled MEMS Microsensor and Actuators, a synthesis was made from specialized literature concerning the structures of MEMS and sensors.

The structures investigated in this work were presented in detail: SAW devices with applications in the field of sensors (Chap.3), electro-thermal actuators, radiofrequency microswitches and cantilevers with applications in the field of vibration sensors. Another important part of this chapter consists of the presentation of MEMS devices based on silicon carbide and their manufacturing technology. Emphasis was placed on the properties of silicon carbide, a special attention being allocated to thermal conductivity, to the high hardness and excellent chemical behaviour in corrosive environments. These properties recommend the use of this semiconductor in manufacturing of MEMS devices and structures with various applications.

In Chapter 3, titled SAW Devices with Applications in the Field of Chemical Sensors, the first original results were presented. It is described the fabrication of a chemical sensor on a $LiTaO_3$. In order to achieve this sensor, we started with a configuration of the delay line and we have first designed the photolithographic masks, since these are the elements that are forming the shape of the final structures and are outlining the stages of technological flow. These 3 photolithographic masks were used for fabricating the delay line, for detection zone generation and for creating the access to the devices contacting pads. Throughout the fabrication stage of the surface acoustic wave (SAW) devices, ***optimal technological solutions for substrate processing have been found***. These solutions are meant to make profit over the excellent piezoelectric properties of the substrate, but in the same time to avoid the undesired accompanying pyroelectric effect. The detecting area of the sensor was made from a gold film, thus comprising ***a good immobilization of antibodies***, while the silicon dioxide has ensured the trapping of the surface acoustic waves on the surface of the piezoelectric material, being a suitable waveguide. The obtained devices were then encapsulated and in order to characterize them, specific ***structures for measurement and calibration have been designed and fabricated***. A functional testing of the sensor was done, and– by use of VNA - it was established how the phase shift of the sensor transfer function is depending on mycotoxin solution concentration. At the end of this chapter the ***sensitivity of the SAW chemical sensor*** was measured and it was found to be $S=0,228^{o}/nM$. This value underlines the high sensitivity of the manufactured devices as a function of even small variation of mycotoxin quantity.

Chapter 4 is devoted entirely to the Fabrication of the MEMS Devices for Vibration Sensors and Microwaves. There were designed, manufactured and tested three distinct types of MEMS devices:

Thermos-electric actuators, RF-MEMS switches and cantilevers. The common ground of all these structures reside in their fabrication technique.

- The designing of electro-thermal actuators was based, as starting point, on the chevron configuration. The fabrication of the structures involved first the designing of photolithography

masks, and then continued with the deposition and configuration of Al structural material. **The simplicity of the fabrication process is pointing toward a high reproducibility of the devices**. The electrical characterization was done by the use of a SÜSS MicroTec on-wafer testing system, Model PM5. **A displacement of 12 μm was measured when a voltage of 0.2 V and a current of 250 mA were applied**.

- The second part of the chapter is dedicated to the fabrication of RF-MEMS switches with electro-thermal actuation. The ***functional bandwidth of the devices was optimized for a maximal frequency of 10 GHz***. The switch configuration comprises two parts: (i) the actuating mechanism that incorporate the driving mechanism, and (ii) the microwave system containing the coplanar waveguides (CPW). The fabrication of the devices started with the designing of 3 photolithography masks used to pattern the SU8 switch and for defining the Cr/Au metallic resistors. The technological steps involved the deposition of two SU8 polymer layers, containing inserted electrical resistors. ***This arrangement is preventing the out-of-plane movement of the suspended structure and it provides a good isolation***. The obtained structures were electrically tested using SÜSS MicroTec on-wafer testing system, Model PM5. Future development perspectives on this device include its microwave testing and the design of a bi-stable mechanism.

- The last part of this chapter is focused on the Technology of Polysilicon fabricated Cantilevers that are used on a wide scale in MEMS devices. An important section of this last part, achieved before the design and fabrication of the cantilevers itself, consisted in ***a study regarding the material structural properties***. Particular attention has been paid to find the proper parameters for deposition of the structural material. In this respect, ***there were realised depositions*** of 2 μm thickness of ***polysilicon layers at four different temperatures: 580^{o}C, 610^{o}C, 630^{o}C and 650^{o}C***, all at a pressure of 2 mbar. It has been observed that ***with the increase in the deposition temperature of the polysilicon layer***, the grain sizes ***grow.*** The average size of ***the grains*** corresponding to the samples obtained ***at 580^{o}C is around 190 nm,*** while the dimensions of those obtained at 650^{o}C are in the range of 750-800 nm. For the ***polysilicon deposited at 580°C***, ***a degree of crystallinity of 97.48% was obtained, while for layers deposited at higher temperatures it was 100%.*** The average ***Young's modulus was evaluated at 140 GPa*** for all cases, except for the polysilicon sample obtained at 580^{o}C, that displayed a value of ***130 GPa for Young's modulus***. In the final part of the chapter we presented the workflow necessary for cantilevers fabrications, which involved a number of 3 photolithography masks. The masks had the purpose of obtaining the actuation electrode, the window opening in the SiO_2 layer in the pad region, in order to facilitate the deposition of the next polysilicon layer, configured with the final photolithography mask for the fabrication of the cantilevers. The manufacturing technology involved successive deposits of polysilicon, doping of the layers and the use of SiO_2 as a sacrificial layer. Electrical characterization of structures showed that a microcantilever with the width of 10 μm and length of 45 μm has an actuating voltage of 205 V.
- ***In Chapter 5***, titled Processes on SiC, there were discussed the key technology of silicon carbide microprocessing in order to obtain MEMS devices on this material. Particular attention was paid to thermal oxidation and dry etching processes. It has been found that ***the thermal oxidation of silicon carbide is much slower than that of Si***.

The etching of 4H-SiC was performed in the coupled capacitive ***RIE reactor***, in the presence of ***a mixture of SF_6 and O_2***. To avoid the micro-masking effect, the mask material was chosen as nickel silicide which is more resistant to plasma at the used specific parameters.

A series of dry etching processes of SiC were performed, aiming at increasing the etching rate and at the same time obtaining a smooth surface. The best results were obtained using a radio-frequency power of 250 W, a pressure of 10 Pa, a S_{F6} flow of 15 sccm (cm^3/min) and an O_2 of 6 sccm. The surface etched with this recipe was smoother, resulting in an ***etching rate of 50.78 nm/min***. These results are promising for the manufacturing of MEMS devices on SiC.

Original contributions

The development of micro-electro-mechanical structures and chemical sensors based on surface acoustic waves devices presented in this thesis was based both on investigations of the fundamental operating mechanisms and on the proposal of optimal configurations and the elaboration of technological processes suitable to the materials and proposed applications, ultimately leading to significant improvements in the operating parameters of the structures. The results obtained have been confirmed in some publications and scientific manifestations and will be presented briefly in this subchapter:

- ***Highlight the importance of the chosen topic:***
  - Placing it in the current context of the SAW and MEMS sensor industry
- ***Syntheses from the literature on:***
  - SAW devices for applications in the field of chemical sensors
  - MEMS structures with electro-thermal and electrostatic actuation
  - Microprocessing of SiC and optimal material selection for masking in the etching process
- ***Photolithography masks Design for the development of chemical sensors and MEMS structures:***
  - Surface acoustic waves structures (SAW) [7, 9]
  - Chevron type electro-thermal actuators [6, 10, 11]
  - RF switches with electro-thermal actuation [15]
  - Microcantilevers with electrostatic actuation [1]
- ***Fabrication processes developing that ensures high reproducibility for a range of MEMS structures and chemical sensors:***
  - Chevron type electro-thermal actuators [6, 10, 11]
  - RF switches with electro-thermal actuation
  - Microcantilevers with electrostatic actuation [1]
  - Chemical sensors based on SAW structures [7, 9]
  - SiC microprocessing
- ***Technological optimizations for a range of innovative devices and materials:***
  - Adaptation of manufacturing technology of SAW chemical sensor to material properties ($LiTaO_3$), using low temperatures of chemical cleaning solutions, which have led to the avoidance of undesirable effects that may occur due to the pyroelectric properties of the substrate.
  - Evaporation of the metal used for configuring the interdigitated structure was achieved by maintaining the substrate at low temperatures [8, 9]
  - The technological development of Chevron's electro-thermal actuators has been aimed at using relatively simple manufacturing processes to ensure high structure reproducibility and compatibility with general semiconductor processes for easy integration with other devices. [6, 10, 11]

- The technological manufacturing flow of RF-MEMS structures was based on the use of two layers of polymeric SU8, inside of which the metal resistors were placed. This solution provided the in-plan movement (parallel to the substrate) of the mobile structure of the actuator
- The deposition of polysilicon layers at low temperatures has resulted in low roughness. Improving the crystallinity and roughness of the polysilicon films was achieved by performing thermal treatments in an atmosphere of N_2
- The morphological characterization results (XRD, AFM and SEM) of the structural materials led to the optimization of the design and manufacturing processes, which subsequently ensured the stability and reliability of the investigated devices in this paper [2- 5], [12-14], [16]
- The optimization of silicon carbide microprocessing methods comprises a series of technological tests, the results in suitable etching rates and smooth etching surfaces

- ***Packaging and characterization procedures for chemical sensors and MEMS devices:***

- Carry out the encapsulation process of the chemical sensors and carry out the calibration kit of the network vector analyzer used for the functional testing of the devices. Microwave testing of obtained devices [8, 9]
- Electrical and IR testing of chevron electro-thermal actuators [11]
- Electrical testing of microcantilevers

List of original papers

ISI international publications:

1. *Voicu, Rodica-Cristina; Gavrila, Raluca; Obreja, Alexandru Cosmin;* ***Baracu, Angela-Mihaela****; Dinescu, Adrian; Müller, Raluca,* Design, microfabrication and analysis of polysilicon thin layers for MEMS vibrating structures, **Analog Integrated Circuits and Signal Processing**, Volume: 82 Issue: 3 Special Issue: SI Pages: 611-620, MAR 2015.
2. *F. Rusu, M. Pustan, C. Birleanu, R. Muller, R. Voicu,* ***A. Baracu,*** Analysis of the surface effects on adhesion in MEMS structures using atomic force microscope, **Applied Surface Science** 358 (2015): 634-640.
3. *R. Voicu ,* ***A. Baracu****, R. Gavrila , C. Obreja , M. Danila, A. Dinescu , B. Bita, R. Müller,* Material Characterizations for MEMS Vibration Sensors and Biostructures Applications, **Digest Journal of Nanomaterials and Biostructures**, Vol. 10, No. 3, 2015, p. 1077 – 1085.
4. *R. Voicu, M. Pustan, C. Birleanu,* ***A. Baracu****, R. Müller,* Mechanical and tribological properties of thin films under changes of temperature conditions, **Surface & Coatings Technology**, Volume: 271 Pages: 48-56 Published: JUN 15, 2015.
5. *Corina Birleanu , Marius Pustan , Raluca Müller , Cristian Dudescu, Violeta Merie, Rodica Voicu,* ***Angela Baracu****,* Experimental investigation by atomic force microscopy on mechanical and tribological properties of thin films**, International Journal of Materials Research**, DOI 10.3139/146.111358, 107 (2016) E; page 1–10.
6. *Marius Pustan, Radu Chiorean, Corina Birleanu, Cristian Dudescu, Raluca Müller,* ***Angela Baracu****, Rodica Voicu,* Reliability Design of Thermally Actuated MEMS switches supported by V –Beams, Microsystem Technologies, pp.1-9, Springer, 2016.

Papers in international conference ISI proceedings

7. ***Angela Baracu****, Monica Nedelcu, Florea Craciunoiu, Rodica Voicu, Raluca Müller,* SH-SAW sensor on Langasite for mass detection in liquid media, International Semiconductor Conference (CAS), **IEEE CAS Proceedings**, Vol.:1, Pp. 115–118, 2013.
8. ***A. Baracu,*** *R. Pascu, F. Craciunoiu,* Ordered shapes of the CVD SiO_2 evidenced by wet etching**,** International Semiconductor Conference, **IEEE CAS Proceedings**, pp. 121 – 124, 2014.
9. ***A. Baracu,*** *A-M. Gurban, I. Giangu, F. Craciunoiu, V. Buiculescu, A. Dinescu, R. Müller, L. Rotariu, C. Bala, C. Mitrea,* Selective Chemical Sensor for Liquid Specimens Based on Lithium Tantalate Surface Acoustic Wave Devices, **IEEE CAS Proceedings**, pp. 271 – 274, 2015 –**Best paper award**.

Papers presented in other conferences:

10. *Rodica-Cristina Voicu, Raluca Müller,* ***Angela Baracu****, Catalin Tibeica, Corina Barleanu, Marius Pustan,* Electro-Thermal Actuators for Space and Micro-Nano Biomanipulation Applications, *NEMS-2014*, Paris, France, 2014, **Book of Abstracts**.
11. ***Angela Baracu****, Rodica Voicu, Raluca Müller, Andrei Avram, Marius Pustan, Radu Chiorean, Corina Birleanu, Cristian Dudescu,* Design and fabrication of a MEMS chevron-type thermal actuator, **AIP Conference Proceedings** 1646, 25 (2015).
12. *M. Michałowski, Z.Rymuza, R.Voicu, A.Obreja,* ***A.Baracu****, R.Muller,* Nanotribological Behaviour of Polysilicon Films Applied in MEMS Devices, **Proceedings of the SAIT Tribology Conference Tribology**, ISBN 978-0-60543-4, South Africa.
13. *Marcin Michalowski, Zygmunt Rymuza, Rodica Voicu, Cosmin Obreja,* ***Angela Baracu****, Raluca Muller,* Control of tribological properties of ultrathin polysilicon films,

Design, Test, Integration and Packaging of MEMS/MOEMS, 2016 Symposium on. **IEEE Proceedings**.

14. *Marcin Michałowski, Zygmunt Rymuza, Rodica Voicu, Cosmin Obreja,* ***Angela Baracu****, Raluca Muller,* Adhesive and frictional properties of ultrathin polysilicon films, 1st international conference on tribology, **Conference Proceedings**, Istanbul – Turkey, 2015.
15. ***Angela Baracu****, Valentin Buiculescu , George Boldeiu, Raluca Müller,* Reliable Design of Thermally Actuated RF-MEMS Switch for Operation in Low-Gigahertz Band, Smart Systems Integration Conference, Cork, Ireland, ***Conference Proceedings***, pp. 355-358, 2017.

Publications in books:

16. *Marcin Michalowski, Zygmunt Rymuza, Rodica Voicu, Cosmin Obreja,* ***Angela Baracu,*** *Raluca Müller,* AFM studies of stiction properties of ultrathin polysilicon films, *in:* **Advanced Mechatronics Solutions**, Ryszard Jablonski and Tomas Brezina Editors, series Advances in Intelligent Systems and Computings vol. 393, Springer International Publishing Switzerland 2016, pp.347-353.

Perspectives for further development

Starting from research on the manufacture and characterization of chemical sensors and MEMS devices, their electrical performance can be improved by optimizing the process and encapsulation techniques of the final devices.

In the future, it will be attempted to improve the sensitivity of the SH-SAW chemical sensor by increasing the contact surface with the liquid sample or by replacing the SiO_2 guiding layer with a Zinc oxide (ZnO). With respect to the packaging part of the devices, the cell used to adapt the sensor to the liquid medium could be replaced by microfluidic channels, designed and fabricated on the same chip with the sensor. The structural material of the microfluidic channels could be the SU8 polymer, in the process of which we have already accumulated experience.

In the case of the RF-MEMS switches, future development perspectives include testing devices in a broadband and the design of a bi-stable mechanism. It has been considered that a bi-stable structure brings important advantages to the operation of the circuit as the drive signal has a low duration, so the power consumption is reduced and no special elements of "locking" of the working positions are required, which reduces the area of the whole circuit due to the limitation of its complexity.

Last but not the least, the development of the etching recipe of SiC (number 7) will be performed in order to obtain a smooth surface. Once this goal has been achieved, the whole suite of technological processes could be used to develop high-temperature SiC sensors or even electronic devices.

REFERENCES

(selection)

[1] *Strutt J W*. On waves propagated along the plane surface of an elastic solid. Proceedings of the London Mathematical Society, 1885, 17(1): 4

[2] *White R M, Voltmer F W.* Direct piezoelectric coupling to surface elastic waves. Appl Phys Lett, 1965, 7(12): 314

[3] *Bill Drafts*, Acoustic Wave Technology Sensors, Sensors Online, Oct 1, 2000.

[4] *Charles S. Smith*, Piezoresistance Effect in Germanium and Silicon, Phys. Rev. 94, 42 – Published 1 April 1954.

[5] *Kerstin Länge, Bastian E. Rapp, Michael Rapp,* Surface acoustic wave biosensors: a review, Analytical and Bioanalytical Chemistry, Volume 391, Issue 5, pp 1509–1519, 2008.

[6] *US patent 3590343, Nathanson et al, "Resonant gate transistor with fixed position electronically floating gate electrode in addition to resonant member", issued 1971-6-29*

[7] "MicroElectroMechanical Systems (MEMS)". ProQuest. October 2001. Retrieved 25 December 2010.

[8] ***A. Baracu****; M. Gurban; I. Giangu; F. Craciunoiu; V. Buiculescu; A. Dinescu; R. Müller; L. Rotariu; C. Bala; C. Mitrea*, Selective chemical sensor for liquid specimens based on lithium tantalate surface acoustic wave devices, Semiconductor Conference (CAS), 2015 International, Pages 271 – 274, DOI: 10.1109/SMICND.2015.7355229.

[9] http://www.wieweb.com/ns6/index.html

[10] ***Angela Baracu****, et al.* Tehnici de proiectare şi fabricare a dispozitivelor cu unde acustice de suprafaţă, Raport de cercetare în cadrul proiectului: Sensing platforms integrating biomimic systems for rapid screening of undesirable substances in food"-Contract prestări servicii IMT-RQ Nr. 107/2012, 2016.

[11] *Chang, Ren-Chuan, et al.*, A study of Love wave devices in ZnO/Quartz and ZnO/$LiTaO_3$ structures." Thin Solid Films 498.1 (2006): 146-151.

[12] *Hong Li, Doug Eng, Chi Tang, P. Westbrook*, "Low dielectric glass fibre development – new printed circuit board base materials", Glass Technology: European Journal of Glass Science and Technology, Part A, vol. 54, no. 2, Aprilie 2013, pp. 81-85

[13] *Zeinab Ramshani, Avuthu S.G. Reddy, Binu B. Narakathu, Jared T.Wabeke, Sherine O. Obare, and Massood Z. Atashbar*, SH-SAW sensor based microfluidic system for the detection of heavy metal compounds in liquid environments, , Sensors and Actuators B: Chemical, 217 (2015) Pages: 72–77.

[14] *G. Lojewski*, Dispozitive şi circuite de microunde, Editura Tehnică, Bucureşti 2005, ISBN 973-31-2263-7.

[15] *B. C. Wadell*, "Transmission line design handbook", Artech House, 1991, ISBN 0-89006-436-9.

[16] *Yong Zhu, Member, IEEE, S. O. Reza Moheimani, Fellow, IEEE, and Mehmet Rasit Yuce, Senior Member, IEEE*, Bidirectional Electrothermal Actuator With Z-Shaped Beams, IEEE SENSORS JOURNAL, VOL. 12, NO. 7, JULY 2012.

[17] *Neha Jain, Anurekha Sharma, Sandeep Kumar,* Design and Simulation of Bidirectional In-Plane Chevron Beam Microtweezer, International Journal of Emerging Technologies in Computational and Applied Sciences, 3(1), pp. 43-49, 2013.

[18] ***Angela Baracu****, Rodica Voicu, Raluca Müller, Andrei Avram, Marius Pustan, Radu Chiorean, Corina Birleanu, Cristian Dudescu,* Design and fabrication of a MEMS chevron-type thermal actuator, 11th International Conference on Nanoscience&Nanotechnologies (NN14), Abstract Book, pp. 181 (2014).

[19] *Giuseppe Schiavone, Marc P. Y. Desmulliez and Anthony J. Walton*, Integrated Magnetic MEMS Relays: Status of the Technology, Micromachines, 5, 2014.

[20] ***Angela Baracu****, Valentin Buiculescu, George Boldeiu, Raluca Müller,* Reliable Design of Thermally Actuated RF-MEMS Switch for Operation in Low-Gigahertz Band, Smart Systems Integration Conference, Cork, Ireland, Conference Proceedings, pp. 355-358, 2017.

[21] *Raluca Müller, Rodica Voicu,* ***Angela Baracu****, Raluca Gavrila, Cosmin Obreja,* Scientific Report, MNT.ERA-Net- 3-Scale modelling for robust-design of vibrating micro sensors, 2015

[22] *R.-C. Voicu, R. Gavrila, A.C. Obreja,* ***A.-M. Baracu****, A. Dinescu, R. Muller,* Design, microfabrication and analysis of polysilicon thin layers for MEMS vibrating structures, Analog Integr Circ Sig Process 82 3 SI, pp. 611-620, (2015).

[23] J.F. Michaud, S. Jiao, A.E. Bazin, M. Portail, T. Chassagne, M. Zielinski and D. Alquier. Micromachining of thin 3C-SiC films for mechanical properties investigation. Materials Research Society Symposium Proceedings 1246 (2010) 213.